5SM

Global Carbon and Other Biogeochemical Cycles and Feedbacks

Supplementary Material

Coordinating Lead Authors:
Josep G. Canadell (Australia), Pedro M.S. Monteiro (South Africa)

Lead Authors:
Marcos H. Costa (Brazil), Leticia Cotrim da Cunha (Brazil), Peter M. Cox (United Kingdom), Alexey V. Eliseev (Russian Federation), Stephanie Henson (United Kingdom), Masao Ishii (Japan), Samuel Jaccard (Switzerland), Charles Koven (United States of America), Annalea Lohila (Finland), Prabir K. Patra (Japan/India), Shilong Piao (China), Joeri Rogelj (United Kingdom/Belgium), Stephen Syampungani (Zambia), Sönke Zaehle (Germany), Kirsten Zickfeld (Canada/Germany)

Contributing Authors:
Georgii A. Alexandrov (Russian Federation), Govindasamy Bala (India/United States of America), Laurent Bopp (France), Lena Boysen (Germany), Long Cao (China), Naveen Chandra (Japan/India), Philippe Ciais (France), Sergey N. Denisov (Russian Federation), Frank J. Dentener (EU, The Netherlands), Hervé Douville (France), Amanda Fay (United States of America), Piers Forster (United Kingdom), Baylor Fox-Kemper (United States of America), Pierre Friedlingstein (United Kingdom), Weiwei Fu (United States of America/China), Sabine Fuss (Germany), Véronique Garçon (France), Bettina Gier (Germany), Nathan P. Gillett (Canada), Luke Gregor (Switzerland/South Africa), Karsten Haustein (United Kingdom/Germany), Vanessa Haverd (Australia), Jian He (United States of America/China), Helene T. Hewitt (United Kingdom), Forrest M. Hoffman (United States of America), Tatiana Ilyina (Germany), Robert B. Jackson (United States of America), Christopher Jones (United Kingdom), David P. Keller (Germany/United States of America), Lester Kwiatkowski (France/United Kingdom), Robin D. Lamboll (United Kingdom/United States of America, United Kingdom), Xin Lan (United States of America/China), Charlotte Laufkötter (Switzerland/Germany), Corinne Le Quéré (United Kingdom), Andrew Lenton (Australia), Jared Lewis (Australia/New Zealand), Spencer Liddicoat (United Kingdom), Laura Lorenzoni (United States of America/Venezuela), Nicole Lovenduski (United States of America), Andrew H. MacDougall (Canada), Sabine Mathesius (Canada/Germany), H. Damon Matthews (Canada), Malte Meinshausen (Australia/Germany), Igor I. Mokhov (Russian Federation), Vaishali Naik (United States of America), Zebedee R. J. Nicholls (Australia), Intan Suci Nurhati (Indonesia), Michael O'Sullivan (United Kingdom), Glen Peters (Norway), Julia Pongratz (Germany), Benjamin Poulter (United States of America),

Jean-Baptiste Sallée (France), Marielle Saunois (France), Edward A.G. Schuur (United States of America), Sonia I. Seneviratne (Switzerland), Ann Stavert (Australia), Parvadha Suntharalingam (United Kingdom/United States of America), Kaoru Tachiiri (Japan), Jens Terhaar (Switzerland/Germany), Rona Thompson (Norway, Luxembourg/New Zealand), Hanqin Tian (United States of America), Jocelyn Turnbull (New Zealand), Sergio M. Vicente-Serrano (Spain), Xuhui Wang (China), Rik Wanninkhof (United States of America), Philip Williamson (United Kingdom)

Review Editors:
Victor Brovkin (Germany/Russian Federation), Richard A. Feely (United States of America)

Chapter Scientist:
Alice D. Lebehot (South Africa/France)

This supplementary material should be cited as:
Canadell, J.G., P.M.S. Monteiro, M.H. Costa, L. Cotrim da Cunha, P.M. Cox, A.V. Eliseev, S. Henson, M. Ishii, S. Jaccard, C. Koven, A. Lohila, P.K. Patra, S. Piao, J. Rogelj, S. Syampungani, S. Zaehle, and K. Zickfeld, 2021: Global Carbon and other Biogeochemical Cycles and Feedbacks Supplementary Material. In *Climate Change 2021: The Physical Science Basis. Contribution of Working Group I to the Sixth Assessment Report of the Intergovernmental Panel on Climate Change* [Masson-Delmotte, V., P. Zhai, A. Pirani, S.L. Connors, C. Péan, S. Berger, N. Caud, Y. Chen, L. Goldfarb, M.I. Gomis, M. Huang, K. Leitzell, E. Lonnoy, J.B.R. Matthews, T.K. Maycock, T. Waterfield, O. Yelekçi, R. Yu, and B. Zhou (eds.)]. Available from https://www.ipcc.ch/

Table of Contents

5.SM.1 Assessment of Recent Advances in Observational and Modelling Methodologies

Since AR5 three major advances have had a decisive impact on the levels of confidence of the trends and the variability of both air–sea fluxes of CO_2 and its storage in the ocean interior. These are (i) the new observations and observational-based products for decadal variability in ocean uptake fluxes and ocean storage, (ii) the observational-based product changes in amplitude of the seasonal cycle of surface ocean pCO_2 (the partial pressure of CO_2 expressed in matm) in response to changing ocean carbonate chemistry, and (iii) spatially resolved pCO_2 seasonal climatologies for the global coastal ocean (Rödenbeck et al., 2015; Landschützer et al., 2016, 2018; Laruelle et al., 2017). These advances were made possible by the simultaneous global coordination of observations and data quality control through the surface ocean CO_2 atlas (SOCAT) and Lamont-Doherty Earth observatory (LDEO), as well as the rapid adoption of a large variety of interpolation techniques for the surface layer and their intercomparison to constrain uncertainties and biases (Rödenbeck et al., 2015; Bakker et al., 2016; Landschützer et al., 2016; McKinley et al., 2017; Gregor et al., 2019; Gruber et al., 2019b).

Advances in the multiple methods of interpolating surface ocean pCO_2 observations provide a *medium* to *high confidence* in the air–sea fluxes of CO_2 over most of the ocean (Rödenbeck et al., 2015; Landschützer et al., 2016; Gregor et al., 2019). However, there is *low confidence* in those fluxes for important regions such as the Southern Ocean, the Arctic and South Pacific, as well as coastal oceans (Laruelle et al., 2017; Gregor et al., 2019; Gruber et al., 2019a); while these regions remain temporally and spatially undersampled, the development and deployment of carbon and biogeochemically enabled Argo autonomous floats is starting to close those gaps (Williams et al., 2017; Gray et al., 2018; Claustre et al., 2020).

Similarly, for anthropogenic carbon storage in the ocean interior (i.e., below the mixed layer) the global ocean ship-based hydrographic investigations programme (GO-SHIP) coupled to the global ocean data analysis project for carbon (GLODAPv2) were central to supporting the advances in characterizing changes to the storage in the ocean interior by generating a new consistent, quality-controlled, global dataset, allowing the decadal variability in ocean carbon storage to be quantified (Lauvset et al., 2016; Olsen et al., 2016; Clement and Gruber, 2018; Gruber et al., 2019b). There is *high confidence* that a significant advance since AR5 and SROCC is the improved characterization of the variability of the ocean CO_2 storage trends in space and time, which has notable decadal and regional-scale variability (Tanhua et al., 2017; Gruber et al., 2019b; see also SROCC Chapters 3 and 5).

Since it is also unequivocal that anthropogenic CO_2 taken up from the atmosphere into the ocean surface layer is further transported into the ocean interior through ocean ventilation processes including vertical mixing, diffusion, subduction and meridional overturning circulations (Sallée et al., 2012; Nakano et al., 2015; Bopp et al., 2015; Toyama et al., 2017; Gruber et al., 2019b), the trends as well as the spatial and temporal variability were assessed in an integrated way for both the air–sea flux and storage of anthropogenic CO_2.

5.SM.2 SeaFlux Method: A Four-Step Methodological Approach to Address the First-order Inconsistencies Between the Six Ocean CO_2 Flux Observational-based Products Used in Chapter 5 (Section 5.2.3.1)

Contributors: Amanda Fay and Luke Gregor

5.SM.2.1 Methods

The SeaFlux method is based on six published and widely used observation-based products of surface ocean partial pressure (of CO_2 (pCO_2)) and spans the years 1988–2018 (Gregor and Fay, 2021). These six include three products derived from neural networks (MPI-SOMFFN, CMEMS-FFNN and NIES-FNN), a mixed-layer scheme product (JENA-MLS), a multiple linear regression (JMA-MLR), and a machine-learning ensemble (CSIR-ML6; Supplementary Materials, Table 5.SM.1). These products are included as they have been regularly updated to extend their time period and incorporate additional data that comes with each annual release of the SOCAT database.

Surface pCO_2 observations play a key role in constraining the global ocean carbon sink. This is because variations in surface ocean pCO_2 is the driving force governing the exchange of CO_2 across the air–sea interface, which is commonly described through a bulk formula (Garbe et al., 2014; Wanninkhof, 2014):

$$\text{Flux} = k_w \cdot sol \cdot (p\text{CO}_2 - p\text{CO}_2^{\text{atm}}) \cdot (1 - ice) \quad (5.\text{SM}.2.1)$$

where *kw* is the gas transfer velocity, *sol* is the solubility of CO_2 in seawater, in units mol m^{-3} μatm^{-1}, pCO_2 is the partial pressure of surface ocean CO_2 in µatm, and pCO^{atm} in units of µatm represents the partial pressure of atmospheric CO_2 in the marine boundary layer. Finally, to account for the seasonal ice cover in high latitudes the fluxes are weighted by 1 minus the ice fraction (*ice*; i.e., the open ocean fraction).

All of these methods provide full three-dimensional fields (latitude, longitude and time) of the sea surface partial pressure of CO_2 (pCO_2) and the air–sea CO_2 flux. In their original form each product may utilize different choices for the inputs to Equation 1. In this work, the fluxes were recomputed using the following inputs to the bulk parametrization approach Equation 1: *kw* is the gas transfer velocity, *sol* is the solubility of CO_2 in seawater, in units mol m^{-3} μatm^{-1}, calculated using the formulation by Weiss (1974), EN4 salinity (Good et al., 2013), Operational Sea Surface Temperature and Sea Ice Analysis (OSTIA) sea surface temperature (Good et al., 2020), and European Centre for Medium-Range Weather Forecasts (ECMWF) ERA5 sea level pressure (Hersbach et al., 2020); *ice* is the sea ice fraction from OSTIA (Good et al., 2020); pCO_2 is the partial pressure

of oceanic CO_2 in matm for each observation-based product after filling, and pCO_2atm is the dry air mixing ratio of atmospheric CO_2 (xCO_2) from the ESRL surface marine boundary layer CO_2 product available at https://www.esrl.noaa.gov/gmd/ccgg/mbl/data.php (Dlugokencky and Tans, 2020) multiplied by ERA5 sea level pressure (Hersbach et al., 2020) at monthly resolution, and applying the water vapour correction according to Dickson et al. (2007).

Flux is defined positive upward, that is CO_2 release from the ocean into the atmosphere is positive, and uptake by the ocean is negative. In the following sections we discuss the three steps that have the greatest impact on the inconsistencies between unadjusted flux calculations in the six pCO_2 products and the approach that we utilise for the SeaFlux ensemble product.

5.SM.2.2 Step 1: Area Filling

Machine-learning methods aim to maximize the utility of the existing in situ observations by extrapolation using various proxy variables for processes influencing changes in ocean pCO_2. Extrapolation with these independently observed variables is possible due to the non-linear relationship between pCO_2 in the surface ocean and the proxies that drive these changes.

However, not all of the proxy variables have complete global ocean coverage for all months, so the resulting pCO_2 products are limited by the extent of the proxy variables. Additionally, in coastal regions there is the potential that different relationships of pCO_2 are expected than in the open ocean, thus limiting the extrapolations. In contrast, the mixed-layer scheme (utilized by the JENA-MLS product) does not suffer from such missing areas but does not distinguish between coastal and open ocean. While the area extent of the available air–sea flux estimates varies between products, there are consistent patterns; nearly all products cover the open ocean, whereas larger differences exist in the coverage of coastal regions, shelf seas, marginal seas and the Arctic Ocean. To account for differing area coverage, past studies (Friedlingstein et al., 2019, 2020; Hauck et al., 2020) have adjusted simply by scaling based on the percent of the total ocean area covered by each observation-based product. This does not account for the fact that some areas have CO_2 flux densities that are higher or lower than the global average. Thus, the magnitude of the adjustment by area-scaling is likely an underestimate (McKinley et al., 2020). One specific example is the northern high latitudes where coverage by the six products varies substantially. Similarly, three products provide estimates in marginal seas such as the Mediterranean while the other three products have no reported pCO_2 values here. Shutler et al. (2016) report that subtle differences in regional definitions can cause differences of >10% in the calculated net fluxes.

To address the inconsistent spatial coverage in products we utilize a newly released open and coastal merged climatology product (MPI-ULB-SOMFFN) that is a blend of the coastal ocean SOMFFN mapping method (Laruelle et al., 2017) and the open ocean equivalent (MPI-SOMFFN; Landschützer et al., 2020), but which now includes missing coastal ocean regions, marginal seas and the full Arctic Ocean. For each observationally based product, we fill missing grid cells with a scaled value based on this global-coverage climatology. The scaling accounts for year-to-year changes in pCO_2 in the missing areas (given that the extended MPI-ULB-SOMFFN product is a monthly climatology centred on the year 2006) and is obtained as follows. To extend the open and coastal merged monthly climatology (MPI-ULB-SOMFFN) to 1988–2018, we calculate a global-scaling factor based on the product-based ensemble mean pCO_2 for regions which are covered consistently by all six pCO_2 products. We first mask all pCO_2 products to a common sea mask before taking an ensemble mean (pCO_2^{ens}). Next, we divide this ensemble mean by the MPI-ULB-SOMFFN climatology (pCO_2^{clim}) at monthly 1°-by-1° resolution (Equation 2). The monthly-scaling factor (*sf* pCO_2) is calculated by taking the mean over the spatial dimensions.

The scaling factor calculation can be represented as:

$$\mathrm{sf}_{pCO_2} = \mathrm{mean}_{x,y}\left(\frac{pCO_2^{\mathrm{ens}}}{pCO_2^{\mathrm{clim}}}\right) \quad (5.SM.2.2)$$

where *sfp*CO_2 is the one-dimensional scaling factor (time dimension), pCO_2^{ens} is the ensemble mean of all pCO_2 products at three-dimension, monthly 1°-by-1° resolution, pCO_2^{clim} is the MPI-ULB-SOMFFN climatology, also at three dimensions but limited to just one climatological year. The *x* and *y* indicate that we take the area-weighted average over longitude (*x*) and latitude (*y*) resulting in the monthly scaling value. If a product mean is exactly equal to the climatology mean, the scaling factor is 1. Value ranges from 0.91 to 1.06 over the 31-year time period. The one-dimensional scaling factor is then multiplied by the MPI-ULB-SOMFFN climatology for each spatial point resulting in a three-dimensional scaled filling map. These values are then used to fill in missing grid cells in each observation-based product. Globally, the adjustments are all less than 20% of the total flux, with the mean adjustment for the six products at 9%. In the Northern Hemisphere however, the filling process can drive adjustments of up to 35%. As expected, the observationally based products with more complete spatial coverage tend to have smaller flux adjustments, however the impact on the final CO_2 flux depends on the ΔpCO_2 and the wind speed of the areas being filled. The only product that does not change during this adjustment process is the JENA-MLS mixed-layer scheme-based product (Rödenbeck et al., 2013), which is produced with full spatial coverage and therefore needs no spatial filling.

Our approach is not without its own assumptions and limitations. We rely on a single estimate of the missing pCO_2 in coastal ocean regions, marginal seas and the full Arctic Ocean, given that this is the only publicly available product currently existing. Nevertheless, the fact that common missing areas along coastal regions and marginal seas are reconstructed using specific coastal observations provides a step forward from the linear-scaling approach currently used by the Global Carbon Budget (Friedlingstein et al., 2019, 2020). Further confidence is provided by previous research showing that climatological relevant signals (i.e., mean state and seasonality) are well reconstructed by the MPI-SOMFFN method.

Furthermore, our scaled filling methodology assumes that pCO_2 in the missing ocean regions is increasing at the same rate as the

common area of open-ocean pCO_2 used to calculate the scaling factor. Research from coastal ocean regions and shelf seas reveal that, in spite of a large spatial heterogeneity, this is a reasonable first-order approximation (Laruelle et al., 2017). While our approach has a constant scaling factor for the missing ocean areas regardless of latitude, we acknowledge that this could be improved with increased understanding.

5.SM.2.3 Step 2: Wind Product Selection

One hundred and eighty historical wind speed observations (including measurements from satellites and moored buoys) are aggregated and extrapolated through modelling and data-assimilation systems to create global wind reanalyses. These reanalyses are required to compute air–sea gas exchange. Air–sea flux is commonly parametrised as a function of the gradient of CO_2 between the ocean and the atmosphere with wind speed modulating the rate of the gas exchange (Equation 1). Each of these wind reanalyses has strengths and weaknesses, specifically on regional and seasonal scales (Chaudhuri et al., 2014; Ramon et al., 2019) but all are considered reasonable options by the community (Roobaert et al., 2018). We use three wind reanalysis products for completeness: the Cross-Calibrated Multi-Platform v2 (CCMP2, Atlas et al., 2011), the Japanese 55-year Reanalysis (JRA-55, Kobayashi et al., 2015) and the European Centre for Medium-Range Weather Forecasts (ECMWF) ERA5 (Hersbach et al., 2020). The wind speed (U10) is calculated at the native resolution of each wind product from the u- and v-components of wind.

5.SM.2.4 Step 3: Calculation of Gas Exchange Coefficient

We employ the quadratic wind speed dependence of the gas-transfer velocity (Wanninkhof, 1992) and calculate the piston velocity (*kw*) for each of the wind reanalysis products as:

$$k_W = a \cdot \langle U^2 \rangle \cdot \left(Sc/_{660}\right)^{-0.5} \quad \text{(5.SM.2.3)}$$

where the units of *kw* are in cm h^{-1}, *Sc* is the dimensionless Schmidt number, and $\langle U^2 \rangle$ denotes the second moment of average 10-m height winds (m s^{-1}). We choose the quadratic dependence of the gas-transfer velocity as it is widely accepted and used in the literature (Wanninkhof, 1992). Observational and modelling studies have often suggested that different parametrizations could be more appropriate under specific conditions (Fairaill et al., 2000; Nightingale et al., 2000; McGillis et al., 2001; Krakauer et al., 2006); however, recent direct carbon dioxide flux measurements made in the high latitude Southern Ocean confirm that even in this high-wind environment, a quadratic parametrization fits the observations best (Butterworth and Miller, 2016). Future updates of the SeaFlux product will include options for other parametrizations. We calculate the square of the wind speed at the native resolution of each wind product and then average it to 1°-by-1° monthly resolution. The order of this calculation is important as information is lost when resampling data to lower resolutions because of the concavity of the quadratic function. For example, if the second moment were calculated from time-averaged wind speeds, it would result in an underestimate of the gas-transfer velocity (Sweeney et al., 2007). The resulting second moment is equivalent to $<U^2> = Umean^2 + Ustd^2$ where Umean and Ustd are the temporal mean and standard deviation calculated from the native temporal resolution of U.

In addition to the choice of wind parametrization, large differences in flux can result due to the scaling coefficient of gas transfer (*a*) that is applied when calculating the global mean piston velocity. This constant originates from the gas-exchange process studies (Krakauer et al., 2006; Sweeney et al., 2007; Müller et al., 2008; Naegler, 2009) using observations of radiocarbon data from the GEOSECS and WOCE/JGOFS expeditions (Key et al., 2004). The ^{14}C released from nuclear bomb testing (hence bomb^{14}C) in the mid-twentieth century has since been taken up by the ocean. The number of bomb-^{14}C atoms in the ocean, relative to the pre-bomb ^{14}C, can thus be used as a constraint on the long-term rate of exchange of carbon between the atmosphere and the ocean. A probability distribution of wind speed is used to optimize the coefficient of gas transfer based on these observed natural and bomb-^{14}C invasion rates. This coefficient must be individually calculated and is not consistent for each wind product. Further, the gas-transfer velocity used by the different pCO_2 mapping products are not scaled to the same bomb-^{14}C estimate. The range of the different bomb-^{14}C estimates is within the range of the uncertainty from the associated studies (Naegler, 2009), but the choice would introduce inconsistency that is easily addressed here.

We scale the gas-transfer velocity to a bomb-^{14}C flux estimate of 16.5 cm hr^{-1} as recommended by Naegler (2009). The coefficient (*a*) is calculated for each wind product via a cost function which optimizes the coefficient of gas transfer:

$$a = k_W \cdot \langle U^2 \rangle^{-1} \cdot \left(Sc/_{660}\right)^{0.5} \cdot (1 - ice) \quad \text{(5.SM.2.4)}$$

where parameters are as defined in Equation 3. The units of the coefficient a are (cm h^{-1}) (m s^{-1})$^{-2}$. Global winds from the wind speed products differ and therefore even with the same bomb-^{14}C observations the scaled coefficient (a) can have a 40% range (Wanninkhof, 2014). By determining the optimal a coefficient for each of the reanalysis winds, uncertainty in the global fluxes can be decreased. Our scaled coefficients correspond well with the estimate using the CCMP wind product to estimate a as 0.251. Differences in the coefficient will also result from the time period considered and the definition of global area and ice fraction applied in the calculation.

This scaling of the gas-exchange coefficient (a) for each wind product is an essential, and an inconsistently applied step, that has large implications for air–sea flux estimates. Without individual scaling, and instead utilising a set value for the gas-transfer coefficient (a) regardless of wind product, our results show that calculated global fluxes could be as high as 9% different depending on which pCO_2 and wind reanalysis product is considered (Roobaert et al., 2018).

5.SM.2.5 Step 4: Further Parameters for Flux Calculation

The remaining parameters of Equation 1 are the solubility of CO_2 in seawater (*sol*), the atmospheric partial pressure of CO_2 (pCO_2atm), and the area weighting to account for sea ice cover. While the choices of products used for these parameters can also result in differences in flux estimates, the impacts are much smaller as compared with the parameters discussed above.

Atmospheric pCO_2 is calculated as the product of surface xCO_2 and sea level pressure corrected for the contribution of water vapour pressure. The choice of the sea level pressure product, or the absence of the water vapour correction can have a small, but not insignificant, impact on the calculated fluxes. Additionally, some products utilize the output of an atmospheric CO_2 inversion product (e.g., CarboScope, Rödenbeck et al. (2013, CAMS CO_2 inversion, Chevallier (2013) which can introduce differences in the flux estimate outside of the sources related to a product's surface ocean pCO_2 mapping method. Importantly, we do not advocate that our estimate of pCO_2atm is an improvement over other estimates thereof; rather we provide an estimate of pCO_2atm that has few assumptions and leads to a methodologically consistent estimate of ΔpCO_2. We maintain the same philosophy in our estimates of solubility of CO_2 in seawater and sea ice area weighting and therefore we do not elaborate on them here.

5.SM.3 Biogeophysical Sequestration Potential of Ocean-Based CDR Methods

Ocean fertilization (OF) aims to boost primary production and subsequently organic carbon export by seeding the ocean surface with nutrients, typically in iron-limited areas such as the Southern Ocean or North Pacific. Iron-fertilization experiments have been inconclusive on whether deep-sea carbon sequestration is enhanced Boyd et al. (2007); Yoon et al. (2018), with only one observing an increase in the biological pump below 1000 m (Smetacek et al., 2012), suggesting that the effectiveness of ocean fertilization is low (*medium confidence*). Model simulations (Oschlies et al., 2010a; Keller et al., 2014) suggest that if ocean fertilization is applied continuously in the Southern Ocean under high CO_2-emission scenarios, CO_2 sequestration rates are initially between 2 and 4 PgC yr^{-1}, but then decrease to 0.4 to 1 PgC yr^{-1} after the initial decade, with an 80-year cumulative carbon uptake of 73–90 PgC. Taking the sequestration rates from these model simulations to constitute an upper limit, we assess the maximum biogeophysical sequestration potential of iron fertilization to be 1 PgC yr^{-1} (*low confidence*). Increased productivity in the fertilized areas would result in decreased productivity in unfertilized regions (Oschlies et al., 2010b). The carbonate counter pump could also reduce iron fertilisation-induced carbon sequestration by 6–32% (Salter et al., 2014).

Artificial ocean upwelling (AOUpw) brings nutrient-rich water to the ocean surface to alleviate nutrient limitation of (near-) surface phytoplankton growth and thus boosts primary production and subsequent ocean CO_2 uptake. For AOUpw to be effective at increasing ocean carbon storage, the increased primary production has to result in increased transfer of organic carbon into the deep ocean. AOUpw also returns previously sequestered dissolved inorganic carbon to the surface ocean, thus increasing surface water pCO_2 and decreasing (or potentially negating) atmospheric CO_2 drawdown stimulated by the additional nutrient input. In model simulations (Oschlies et al., 2010b; Keller et al., 2014) where AOUpw is applied continuously and at the largest feasible scales, atmospheric CO_2 removal is up to 4.3 PgC yr^{-1} during the first decade, and decreases afterwards to 0.9 to 1.5 PgC yr^{-1} (average), with an 80-year cumulative CO_2 removal of 80 to 140 PgC. Of this removal, 50–80% results from cooling-induced enhancement of the terrestrial carbon sink (Keller et al., 2014). Removing terrestrial CO_2 removal from the total cumulative CO_2 removal yields cumulative ocean CO_2 removal of 16–70 PgC over 80 years, or 0.2–0.9 PgC yr^{-1} (*low confidence*).

Ocean alkalinization, via the deposition of alkaline minerals (e.g., olivine) or their dissociation products (e.g., quicklime) at the ocean surface, can increase surface total alkalinity and thus increase CO_2 uptake and storage. Modelling studies suggest that massive additions of alkalinity (114 Pmol by the end of the century) in high CO_2 emission scenarios could increase ocean uptake by up to 27 PgC yr^{-1} by the end of the century (cumulative atmospheric CDR of up to 905 PgC), and permanently keep it there (100 ka residence time; Renforth and Henderson, 2017) even if additions were stopped (González and Ilyina, 2016; Feng et al., 2017; Sonntag et al., 2018). Taking the sequestration rates from these model simulations to constitute an upper limit, we assess the maximum biogeophysical sequestration potential of ocean alkalinization to be 10 PgC yr^{-1} (*medium confidence*).

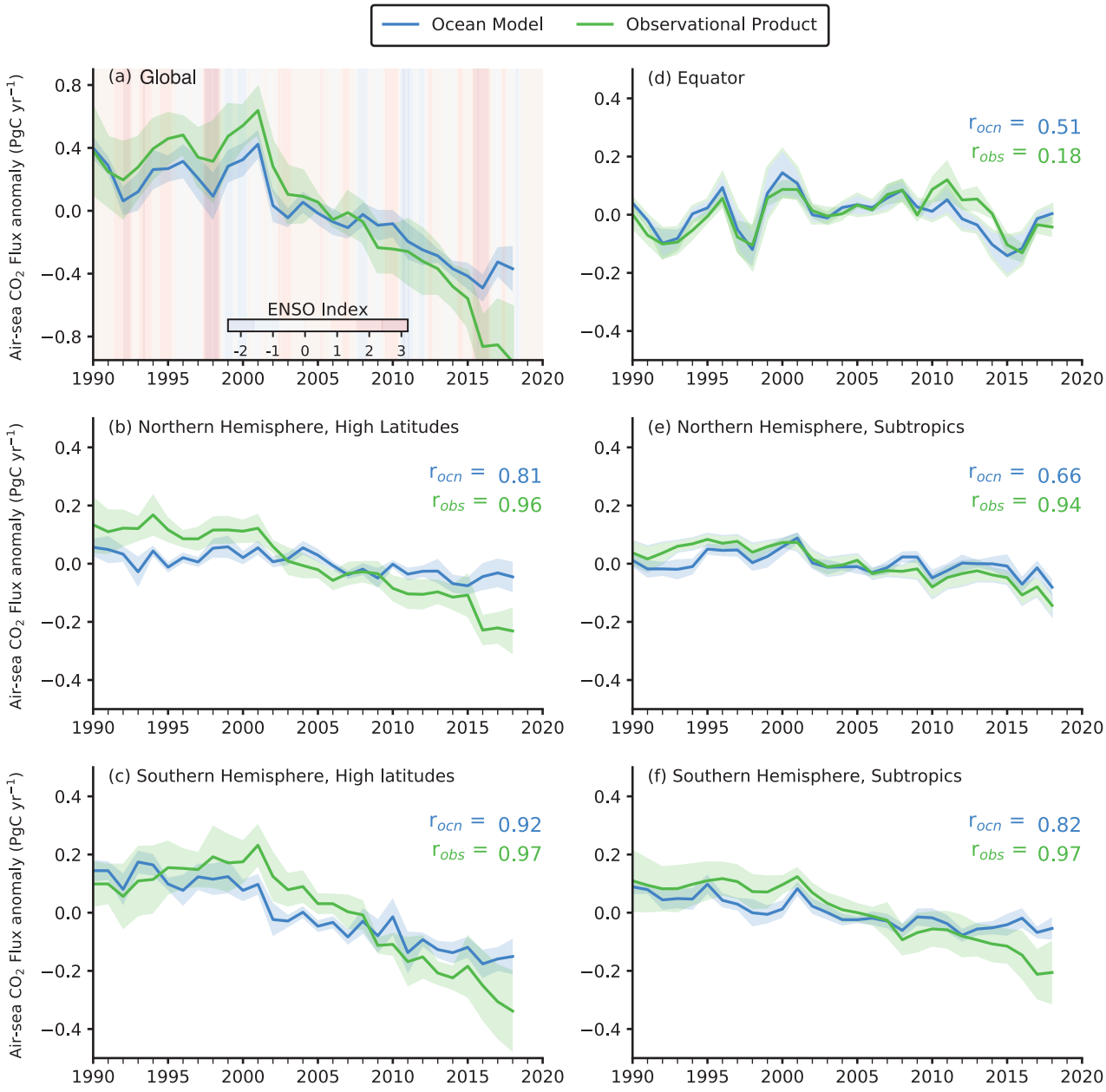

Figure 5.SM.1 | A comparative assessment of the contribution made by five regional ocean biomes (panels b–f) to the temporal variability characteristics of the global mean air–sea CO_2 flux anomalies for the period 1990–2018 using ensembles of global ocean biogeochemical models (GOBMs; nine time series), observation-based products (six time series; Supplementary Material 5.SM.2; Gregor et al. (2019); based on the SOCATv6 observational data, Bakker et al. (2016). Numbers in the top right of panels (b) to (f) indicate the correlation between the regional mean time series of the different models and the global mean time series **(a)**. The five regional super-biomes (boundaries in Figure 5.9a) were derived by aggregation of the original 17 biomes of Fay and McKinley (2014).

Table 5.SM.1 | Decadal mean for the global ocean sink (S_{ocean}) for anthropogenic CO_2 (PgC yr^{-1}) from global ocean biogeochemistry models, pCO_2 observation-based data products, and atmospheric CO_2 inverse models. The uncertainty range for the mean of each approach is 90% confidence intervals. The range of ocean CO_2 uptake for each model or product represents interannual variability.

Methods	1990–1999		2000–2009		2009–2018		2010–2019		Citation
Global Ocean Biogeochemistry Models	**–1.96**	**± 0.48**	**–2.14**	**± 0.54**	**–2.48**	**± 0.56**	**–2.51**	**± 0.56**	
CESM-ETH	–1.81	± 0.26	–1.98	± 0.37	–2.30	± 0.26	–2.35	± 0.29	Doney et al. (2009a)
CSIRO	–2.45	± 0.27	–2.74	± 0.40	–3.10	± 0.24	–3.14	± 0.23	Law et al. (2017)
FESOM-1.4-REcoM2	–1.73	± 0.22	–1.80	± 0.34	–2.13	± 0.36	–2.18	± 0.30	Hauck et al. (2020)
MPIOM-HAMOCC6	–1.67	± 0.19	–1.94	± 0.26	–2.23	± 0.26	–2.25	± 0.26	Paulsen et al. (2017)
NEMO3.6-PISCESv2-gas (CNRM)	–1.90	± 0.27	–1.92	± 0.27	–2.27	± 0.22	–2.31	± 0.25	Berthet et al. (2019)
NEMO-PlankTOM5	–2.14	± 0.25	–2.29	± 0.27	–2.67	± 0.23	–2.71	± 0.20	Buitenhuis et al. (2013)
MICOM-HAMOCC (NorESM-OCv1.2)	–2.39	± 0.20	–2.60	± 0.24	–2.91	± 0.28	–2.95	± 0.24	Schwinger et al. (2016)
MOM6-COBALT (Princeton)	–1.74	± 0.23	–1.97	± 0.43	–2.35	± 0.24	–2.39	± 0.20	Liao et al. (2020)
NEMO-PISCES (IPSL)	–1.85	± 0.26	–2.05	± 0.32	–2.35	± 0.31	–2.35	± 0.31	Aumont et al. (2015)
pCO_2 Observation-based Data Products*	**–1.89**	**± 0.37**	**–2.06**	**± 0.20**	**–2.62**	**± 0.32**			
MPI_SOMFFN	–1.74	± 0.23	–1.93	± 0.38	–2.54	± 0.11			Landschützer et al. (2014)
JENA_MLS	–1.96	± 0.23	–2.12	± 0.31	–2.52	± 0.19			Rödenbeck et al. (2014)
LSCE_FFNN2	–1.77	± 0.05	–1.94	± 0.18	–2.46	± 0.28			Denvil-Sommer et al. (2019)
CSIR_ML6	–1.74	± 0.08	–2.01	± 0.24	–2.57	± 0.20			Gregor et al. (2019)
NIES_NN	–1.80	± 0.10	–2.14	± 0.26	–3.00	± 0.44			Zeng et al. (2014)
JMA_MLR	–2.31	± 0.16	–2.24	± 0.17	–2.66	± 0.29			Iida et al. (2020)
Atmospheric CO_2 inverse Models[a]			**–2.13**	**± 0.47**	**–2.36**	**± 0.72**	**–2.40**	**± 0.74**	
MIROC4-Ir2020			–1.97	± 0.27	–1.91	± 0.45	–1.90	± 0.45	Saeki and Patra (2017)
MIROC4-gcp2020			–1.90	± 0.30	–2.10	± 0.27	–2.18	± 0.31	Saeki and Patra (2017)
CAMS2020			–2.12	± 0.11	–2.54	± 0.23	–2.60	± 0.24	Chevallier et al. (2005)
CTE2020			–2.54	± 0.46	–2.88	± 0.29	–2.91	± 0.26	van der Laan-Luijkx et al. (2017)
Previous IPCC Assessment Reports									
TAR	–1.7	± 0.8							Prentice et al. (2001)
AR4	–2.2	± 0.7							Denman et al. (2007)
AR5	–2.2	± 0.7	–2.3	± 0.7					Ciais et al. (2013)

[a] Pre-industrial sea-to-air CO_2 flux associated with land-to-ocean carbon flux of +0.62 PgC yr^{-1} (Jacobson et al., 2007; Resplandy et al., 2018) has been subtracted from original flux estimates.

Table 5.SM.2 | Decadal means for the global ocean sink (S_{ocean}) for anthropogenic CO_2 (PgC yr^{-1}) from methods additional to those shown in Table 5.SM.1.
The uncertainty ranges presented here are 90% confidence intervals unless otherwise specified.

Methods	Citation	Period	Sea-to-air Flux			Global Ocean Biogeochemistry Models		pCO_2 Observation-based data Products		Atmospheric CO_2 Inverse Models	
Ocean interior carbon inventory change	Gruber et al. (2019b)	1994–2007	–2.23	± 0.31			± 0.50	–1.93	± 0.27	–1.99	± 0.20
Ocean interior CFC inventory change	McNeil et al. (2003)	1980–1989	–1.6	± 0.4	[a]	–1.71	± 0.48				
		1990–1999	–2.0	± 0.4	[a]	–1.96	± 0.48	–1.89	± 0.37		
Ocean interior $\delta^{14}C$ change and GOBMs	Graven et al. (2012)	1990–2007	–2.0	± 0.3	[a]	–2.03	± 0.50	–1.94	± 0.30		
Ocean inverse model	Gloor et al. (2003)	1990	–1.80	± 0.40	[a]	–1.79	± 0.54	–1.87	± 0.60		
	Mikaloff Fletcher et al. (2006); Gruber et al. (2009)	1995–2000	–2.2	± 0.41		–1.94	± 0.47	–1.81	± 0.34	–2.02	± 0.04
	DeVries et al. (2017)	1990–1999	–1.25	± 0.53		–1.96	± 0.48	–1.89	± 0.37		
		2000–2014	–2.41	± 0.20		–2.24	± 0.55	–2.20	± 0.19	–2.21	± 0.35
Joint atmosphere-ocean inversion	Jacobson et al. (2007)	1992–1996	–2.1	± 0.2		–1.99	± 0.45	–1.88	± 0.33		
Deconvolution atm. $\delta^{13}C$ and CO_2	Joos et al. (1999)	1985–1995	–2.0	± 1.3		–1.84	± 0.49				
Atmospheric O_2/N_2 ratio and $\delta^{13}C$	Battle et al. (2000)	1991–1997	–2.0	± 0.6	[a]	–1.97	± 0.47	–1.90	± 0.35		
Air–sea $\delta^{13}C$ disequilibrium	Gruber and Keeling (2001)	1985–1995	–1.5	± 0.9	[a]	–1.84	± 0.49				
Atmospheric O_2/N_2 ratio	Bender et al. (2005)	1994–2002	–1.70	± 0.50	[a]	–1.95	± 0.48	–1.81	± 0.31	–2.01	± 0.06
	Keeling and Manning (2014)	1990–2000	–1.94	± 1.02		–1.95	± 0.48	–1.87	± 0.36		
		1993–2003	–2.20	± 0.94		–1.98	± 0.48	–1.85	± 0.30	–1.96	± 0.13
		2000–2010	–2.72	± 0.99		–2.16	± 0.54	–2.09	± 0.19	–2.12	± 0.31
		1991–2011	–2.45	± 0.96		–2.09	± 0.51	–2.02	± 0.24		
	Tohjima et al. (2019)	1999–2003	–2.20	± 1.20		–1.99	± 0.52	–1.82	± 0.33	–2.06	± 0.11
		2004–2008	–1.97	± 1.02		–2.22	± 0.57	–2.18	± 0.19	–2.17	± 0.45
		2009–2013	–2.65	± 1.44		–2.37	± 0.56	–2.43	± 0.24	–2.26	± 0.48
		2012–2016	–3.05	± 1.49		–2.55	± 0.57	–2.63	± 0.33	–2.40	± 0.39

Table 5.SM.3 | Compiled information on the rates of pH change and aragonite saturation state (Ω_{arag}) change from various time series, ship reoccupations and moorings.

Station, Region		Study Period	pH Change (Per Decade)	Uncertainty	Ω_{arag} Change (Per Decade)	Uncertainty	Study Type	Citation
North Atlantic								
Iceland Sea (68°N, 12.67°W)	(winter)	1985–2008	–0.024	±0.002	–0.072	±0.007	Time series	Olafsson et al. (2009)
		1985–2010	–0.014	±0.005	–0.018	±0.027		Bates et al. (2014)
Irminger Sea (64.3°N, 28°W)		1983–2004	–0.026	±0.006	–0.08	±0.04	Time series	Bates et al. (2014)
Subpolar Gyre		1981–2007	–0.022	±0.004			Merged ship occupations	Lauvset and Gruber (2014)
NA-SPSS		1991–2011	–0.02	±0.004			Merged ship occupations	Lauvset et al. (2015)
NA-STSS		1991–2011	–0.018	±0.003			Merged ship occupations	Lauvset et al. (2015)

Station, Region		Study Period	pH Change (Per Decade)	Uncertainty	Ω_{arag} Change (Per Decade)	Uncertainty	Study Type	Citation
BATS (32°N, 64°W)		1983–2010	–0.018	±0.002	–0.11	±0.01	Time series	Takahashi et al. (2014)
		1983–2012	–0.017	±0.001	–0.095	±0.007		Bates et al. (2014)
		1983–2020	–0.019	±0.001	–0.09	±0.01		Bates and Johnson (2020)
ESTOC (29.04°N, 15.50°W)		1995–2004	–0.017	±0.003			Time series	González-Dávila et al. (2010)
		1995–2011	–0.018	±0.002	–0.115	±0.023		Bates et al. (2014)
		1996–2010	–0.02	±0.004	–0.1	±0.02		Takahashi et al. (2014)
NA-STPS		1991–2011	–0.011	±0.002			Merged ship occupations	Lauvset et al. (2015)
CARIACO (10.50°N, 64.66°W)		1995–2012	–0.025	±0.004	–0.066	±0.028	Time series	Bates et al. (2014)
Mediterranean								
Dyfamed (43.42°N, 7.87°E)		1995–2011	–0.03	±0.01			Time series	Marcellin Yao et al. (2016)
GIFT, Gibraltar		2012–2015	–0.044	±0.006			Time series	Flecha et al. (2019)
Equatorial Atlantic								
A-EQU		1991–2011	–0.016	±0.003			Merged ship occupations	Lauvset et al. (2015)
South Atlantic								
SA-STPS		1991–2011	–0.011	±0.005			Merged ship occupations	Lauvset et al. (2015)
Atlantic Meridional Transect (50°S–50°N)		1995–2013	–0.013	±0.009			Merged ship occupations	Kitidis et al. (2017)
North Pacific								
NP-SPSS		1983–2011	–0.003	±0.005			Merged ship occupations	Lauvset et al. (2015)
		1991–2011	–0.013	±0.005				
Papa (50°N, 145°W)		2007–2014	–0.01	±0.005	0.1	0.04	Mooring	Sutton et al. (2017)
K2 (47°N, 160°E)		1999–2015	–0.025	±0.01	–0.12	0.05	Time series	Wakita et al. (2017)
	(winter)		–0.008	±0.004				
NP-STSS		1991–2011	–0.01	±0.005			Merged ship occupations	Lauvset et al. (2015)
HOT (22.75°N, 158°W)		1988–2007	–0.019	±0.002			Time series	Dore et al. (2009)
		1988–2009	–0.018	±0.001	–0.08	±0.01		Takahashi et al. (2014)
		1988–2011	–0.016	±0.001	–0.084	±0.011		Bates et al. (2014)
WHOTS (23°N, 158°W)		2004–2013	–0.02	±0.003	–0.2	±0.02	Mooring	Sutton et al. (2017)
KEO (32°N, 144°E)		2007–2014	–0.01	±0.005	–0.1	±0.02	Mooring	Sutton et al. (2017)
137°E Line	33°N–34°N	1994–2008	–0.020	±0.007	–0.12	±0.05	Merged ship occupations	Ishii et al. (2011)
	26°N–30°N	1983–2017	–0.0193	±0.0008	–0.121	±0.005	Merged ship occupations	Ono et al. (2019)
	20°N–22°N		–0.0171	±0.0007	–0.113	±0.004		
	11°N–18°N		–0.0136	±0.0007	–0.09	±0.005		
	5°N–10°N		–0.0124	±0.0008	–0.081	±0.005		
NP-STPS		1983–2011	–0.016	±0.002			Merged ship occupations	Lauvset et al. (2015)
		1991–2011	–0.019	±0.002				

Station, Region		Study Period	pH Change (Per Decade)	Uncertainty	Ω_{arag} Change (Per Decade)	Uncertainty	Study Type	Citation
Equatorial Pacific								
WP-EQU		1983–2011	–0.01	±0.002			Merged ship occupations	Lauvset et al. (2015)
		1991–2011	–0.012	±0.002				
Warm Pool in 130°E–180°		1985–2016	–0.013	±0.001	–0.083	±0.007	Merged ship occupations	Ishii et al. (2020)
EP-EQU		1983–2011	–0.023	±0.003			Merged ship occupations	Lauvset et al. (2015)
		1991–2011	–0.026	±0.002				
TAO	0°, 155°W	1997–2011	–0.022	±0.003			Moorings	Sutton et al. (2014)
	0°, 140°W	2004–2011	–0.018	±0.004				
	0°, 125°W	2004–2011	–0.026	±0.005				
South Pacific								
Munida (45.833°S, 171.5°E)		1998–2011	–0.013	±0.003	–0.085	±0.026	Time series	Bates et al. (2014)
SP-STPS		1983–2011	–0.019	±0.002			Merged ship occupations	Lauvset et al. (2015)
		1991–2011	–0.022	±0.003				
Stratus (20°S, 86°W)		2006–2015	–0.02	±0.003	–0.1	±0.03	Merged ship occupations	Sutton et al. (2017)
Indian Ocean								
East Eq. Indian (90°E–95°E)		1962–2012	–0.016	±0.001	–0.095	±0.005	Merged ship occupations	Xue et al. (2014)
IO-STPS		1987–2011	–0.024	±0.004			Merged ship occupations	Lauvset et al. (2015)
		1991–2011	–0.027	±0.005				
Southern Ocean								
140°E–160°E	North of STF	1969–2003	–0.011	±0.004			Merged ship occupations	Midorikawa et al. (2012)
	SAZ		–0.011	±0.004				
	PFZ		–0.013	±0.003				
	PZ		–0.020	±0.003				
Drake Passage	SAZ	2002–2012	–0.023	±0.007	–0.09	±0.05	Merged ship occupations	Takahashi et al. (2014)
	PZ		–0.015	±0.008	–0.06	±0.05		
SO-STSS		1983–2011	–0.006	±0.004			Merged ship occupations	Lauvset et al. (2015)
		1991–2011	–0.004	±0.004				
SO-SPSS		1983–2011	–0.02	±0.002			Merged ship occupations	Lauvset et al. (2015)
		1991–2011	–0.021	±0.002				
PAL-LTER, West Antarctic Peninsula		1993–2012	0.02	±0.02	0.01	±0.1	Time series	Hauri et al. (2015)
SO-ICE		1991–2011	–0.002	±0.004			Merged ship occupations	Lauvset et al. (2015)

Table 5.SM.4 | Explanation and references of Earth system feedbacks, biogeochemical and biophysical impacts, and trade-offs and co-benefits of the carbon dioxide removal (CDR) methods as presented in Figure 5.37.

CDR Method	Earth System Feedbacks on CO_2 Sequestration Potential and Temperature	Biogeochemical and Biophysical Effects	Trade-offs and Co-benefits Related to Water Quantity and Quality, Food Supply and Biodiversity (BD)
Afforestation, reforestation and forest management	Weakens ocean C sequestration through decreased [CO_2] (Keller et al., 2018; Sonntag et al., 2018); decrease in albedo due to afforestation weakens the effect of CO_2 removal on surface air temperature (Sonntag et al., 2018); may shift the location of the Inter-tropical Convergence Zone and hence precipitation in the monsoon regions (Devaraju et al., 2015a).	Increased emissions of biogenic volatile organic compounds (BVOC; Krause et al. (2017); SRCCL Sections 2.5.2.1 and 2.6.1.2) decreased and increased surface temperature, in the tropics and boreal regions, respectively, due to changes in albedo, evapotranspiration and surface roughness (SRCCL Section 2.5.2.1; Fuss et al., 2018; Griscom et al., 2017; Pongratz et al., 2010; Devaraju et al. (2015b); decreased Chen et al. (2019) or increased (Benanti et al., 2014) N_2O emissions; increased CH_4 uptake Chen et al. (2019).	Threatened water supply in dry areas regional climate, initial land cover, and scale of deployment (Farley et al., 2005; Mengis et al., 2019); improved water quality due to higher soil water retention and filtering capacity (Smith et al., 2019); affects food supply through competition for land (Smith et al., 2018); decreased BD if not adopted wisely, increased BD if monocultures are replaced by native species (Williamson and Bodle, 2016; Smith et al., 2018); potentially negative impacts on food security due to land requirements (Smith et al., 2020).
Soil carbon sequestration	Weakens ocean C sequestration through decreased [CO_2] (Keller et al., 2018).	Decreased or increased N_2O emissions, depending on management strategy, fertilization, land use, use of cover crops (Gu et al., 2017; Fuss et al., 2018). Small or negligible impact on soil CH_4 flux (Smith et al., 2008); Albedo increase by no-till farming (Davin et al., 2014).	Reduced nutrient losses, increased biological activity (Tonitto et al., 2006; Fornara et al., 2011; Paustian et al., 2016), improved soil water holding capacity (Paustian et al., 2019), positive impact on food security due to increased yield (Smith et al., 2020); no impact or increased BD, depending on method (Paustian et al., 2016; Smith et al., 2018).
Biochar	Weakens ocean C sequestration through decreased [CO_2] (Keller et al., 2018).	Decreased N_2O emissions (Cayuela et al., 2014; Kammann et al., 2017), decreased CH_4 uptake in non-inundated soils (Jeffery et al., 2016); decreased CH_4 emissions in inundated soils such as rice fields (Jeffery et al., 2016; Huang et al., 2019; S. Wang et al., 2019; Yang et al., 2019), local warming related to darkened surface (Genesio et al., 2012; Zhang et al., 2018b; Jia et al., 2019, SRCCL); VOC's produced when preparing biochar can be toxic to plants and animals (Buss and Mašek, 2016).	Improved soil fertility and productivity, reduced nutrient losses, enhanced fertiliser N use efficiency (Woolf et al., 2010; Clough et al., 2013; Shen et al., 2016; Liu et al., 2017); improved soil water holding (Karhu et al., 2011; Liu et al., 2016; Bock et al., 2017; Fischer et al., 2019; Verheijen et al., 2019); no impact or increased BD (Smith et al., 2018); adverse impacts on BD due to land requirements of feedstock (12.3.3, WGIII); benefits for food security due to improved yields (Smith et al., 2020).
Peatland restoration	No evidence	Enhanced CH_4 emission (Wilson et al., 2016a); suppressed N_2O emissions (Wilson et al., 2016b); increased (Koskinen et al., 2017) or decreased (Singh et al., 2019) leaching of nutrients; surface cooling due to higher evapotranspiration (Hemes et al., 2018; Worrall et al., 2019; Helbig et al., 2020).	Increased nutrient infiltration and retention to increase water quality (Daneshvar et al., 2017; Kluber et al., 2014); protection from fire, increased BD Meli et al. (2014) Smith et al. (2018).
Restoration of vegetated coastal ecosystems ('blue carbon')	No evidence	Emission of CH_4 and N_2O, and biogenic calcification may partly offset benefits (Rosentreter et al., 2018).	Provision of a very wide range of ecosystem services (biodiversity support recreation and tourism; fishery habitats; improved water quality, and flood and erosion protection; Bindoff et al. (2019).
Ocean fertilization	Carbonate counter pump could decrease C sequestration (Salter et al., 2014); weakens terrestrial C storage (Keller et al., 2018).	Enhanced subsurface ocean acidification (Cao and Caldeira, 2010; Williamson et al., 2012); increased suboxic zone extent in fertilised areas; shrinkage of suboxic zones outside fertilized areas Oschlies et al. (2010a); Mengis et al. (2019); Keller et al. (2014); increased production of N_2O and CH_4 Jin and Gruber (2003).	Perturbation to marine ecosystems via reorganization of community structure, including possibly toxic algal blooms (Oschlies et al., 2010a; Williamson et al., 2012).
Artificial ocean upwelling	Cooling effect; increases terrestrial C storage (Oschlies et al., 2010b; Keller et al., 2014); returns previously sequestered C to ocean surface, decreasing or potentially negating CO_2 drawdown (Bauman et al., 2014; Kwiatkowski et al., 2015).	Enhanced subsurface ocean acidification Williamson et al. (2012); increased suboxic zone extent in fertilized areas Keller et al. (2014); alters ocean temperature, salinity and circulation (Keller et al., 2014); alters Earth's heat and water budget (Keller et al., 2014); increased production of N_2O and CH_4 (Jin and Gruber (2003).	Perturbation to marine ecosystems via reorganisation of community structure, including possibly toxic algal blooms (Oschlies et al., 2010a; Williamson et al., 2012).

CDR Method	Earth System Feedbacks on CO_2 Sequestration Potential and Temperature	Biogeochemical and Biophysical Effects	Trade-offs and Co-benefits Related to Water Quantity and Quality, Food Supply and Biodiversity (BD)
Ocean alkalinization	Increased ocean C storage through enhanced primary production through addition of iron and silicic acid from olivine dissolution (Köhler et al., 2013; Hauck et al., 2016); lowers terrestrial carbon storage (González and should be Ilyina, 2016).	Decreased ocean acidification (surface waters only); decreased deoxygenation (González and Ilyina, 2016).	Release of toxic trace metals from some deposited minerals (Hartmann et al., 2013). Perturbation to marine ecosystems via reorganization of community structure (González and Ilyina, 2016; González et al., 2018).
Enhanced weathering – terrestrial	Will initially reduce the ocean CO_2 sequestration, but after enough weathering products are transported into ocean to increase alkalinity, will increase ocean CO_2 sequestration (Keller et al., 2018).	Decreased N_2O emissions (Kantola et al., 2017; Blanc-Betes et al. 2020); reduced ocean acidification (Beerling et al., 2018).	Soil fertilization and stimulated biological production (Hartmann et al., 2013); can liberate toxic trace metals into soil or water bodies (Keller et al., 2018); can decrease drinking water quality by causing freshwater salinization (Kaushal et al., 2018); increases alkalinity and pH of natural waters (Beerling et al., 2018); adverse impact on BD from mining (Smith et al., 2018).
BECCS	Weakens ocean C sequestration through decreased [CO_2] (Keller et al. 2018); can weaken or strengthen land C sequestration depending on whether bioenergy crops replace marginal land or carbon-rich ecosystems (Don et al., 2012; Heck et al., 2016; Boysen et al., 2017) (Harper et al., 2018).	Increased N_2O emissions related to land use or if fertilized Smith et al. (2016) local warming due to decreased albedo depending on the type of bioenergy crop Smith et al. (2016); VOC emissions (Krause et al., 2017).	Threatened water supply Farley et al. (2005) ; Cross-Chapter Box 5.1) threatened food supply through competition for land (Smith et al., 2019); soil nutrient deficiency; decreased BD depending on scale and previous land-use (Heck et al., 2018; Smith et al., 2018; Creutzig et al., 2019); see DACCS for storage-related side effects.
Direct air carbon capture and storage (DACCS)	Weakens ocean and land C sequestration through decreased [CO_2] (Tokarska and Zickfeld, 2015; Jones et al., 2016; Zickfeld et al., 2021).	No evidence or not applicable	Perturbation of marine ecosystems through leakage of CO_2 from submarine storage (Molari et al., 2018); potentially decreased BD due to land and water requirements (Williamson and Bodle, 2016); water use or production (Fuss et al., 2018; NASEM, 2019); VOC emissions in solid-sorbent systems (NASEM, 2019); storage related: pollution of drinking water; seismic activity, leaks (Fuss et al., 2018).

Table 5.SM.5 | Carbon dioxide removal (CDR) potentials: details underlying sequestration potentials classification shown in Figure 5.37.

CDR Method	Technical/ Biogeophysical Sequestration Potential Class[a]	Confidence Level	Technical/ Biogeophysical Sequestration Potential Median and Range[b]	Sequestration Potential Category	Data Source
Afforestation, reforestation and forest management	Large	Medium (*large evidence, medium agreement*)	Afforestation, reforestation: 3.7 (0.5–10) $GtCO_2e\ yr^{-1}$; forest management 1.8 (1–2.1) $GtCO_2e\ yr^{-1}$	Technical potential; estimates also consider environmental and social factors.	Median and range calculated based on technical and sustainable potentials from Roe et al. (2019).
Soil carbon sequestration	Moderate	Medium (*large evidence, medium agreement*)	Croplands: 1.6 (0.4–6.8) $GtCO_2e\ yr^{-1}$; Pasture lands: 0.7 (0.15–2.6) $GtCO_2e\ yr^{-1}$	Technical potential; estimates also consider environmental and social factors.	Median and range calculated based on technical and sustainable potentials from Roe et al. (2019).
Biochar	Moderate	Medium (*medium evidence, medium agreement*)	1.1 (0.1–4.9) $GtCO_2e\ yr^{-1}$	Technical potential; estimates also consider environmental and social factors.	Median and range calculated based on technical and sustainable potentials from Roe et al., (2019).
Peatland restoration	Moderate	Low (*low evidence*)	0.7 (0.6–0.8) $GtCO_2e\ yr^{-1}$	Technical potential; estimates also consider environmental and social factors.	Median and range calculated based on technical and sustainable potentials from Roe et al. (2019).
Restoration of vegetated coastal ecosystems ('blue carbon')	Low	Low (*low evidence*)	0.2–0.7 $GtCO_2\ yr^{-1}$ (0.05–0.2 $GtC\ yr^{-1}$); 0.2–0.8 $GtCO_2\ yr^{-1}$	Technical potential; estimates also consider environmental and social factors.	SROCC Ch 5 (IPCC, 2019); range calculated based on technical and sustainable potentials from Roe et al. (2019).
Ocean iron fertilization	Large	Low (*medium evidence, low agreement*)	<3.7 $GtCO_2\ yr^{-1}$ (<1 $GtC\ yr^{-1}$); 3.7 $GtCO_2\ yr^{-1}$ (1 $GtC\ yr^{-1}$); 3.7 (0–44) $GtCO_2\ yr^{-1}$	Biogeophysical potential	Supplementary Material 5.SM3; GESAMP (2019); Table 4.4; median and range based on global studies considered in Fuss et al. (2018).
Artificial ocean upwelling	Moderate	Low (*low evidence*)	0.7–3.3 $GtCO_2\ yr^{-1}$ (0.2–0.9 $GtC\ yr^{-1}$); <0.7 $GtCO_2\ yr^{-1}$ (< 0.2 GtC/yr)	Biogeophysical potential	Supplementary Material 5.SM3; GESAMP (2019); Table 4.4.
Ocean alkalinization	Large	Medium (*medium evidence, medium agreement*)	<37 $GtCO_2\ yr^{-1}$ (<10 $GtC\ yr^{-1}$); 3.7 $GtCO_2\ yr^{-1}$ (1 $GtC\ yr^{-1}$); 1–99 $GtCO_2\ yr^{-1}$	Biogeophysical potential	Supplementary Material 5.SM3; GESAMP (2019); Table 4.4; full range (Fuss et al., 2018).
Enhanced weathering	Large	Medium (*medium evidence, low agreement*)	3.7 (1–95) $GtCO_2\ yr^{-1}$	Technical potential	Median and range based on global studies considered in (Fuss et al., 2018) .
BECCS	Large	Medium (*medium evidence, medium agreement*)	4.6 (0.4–11.3) $GtCO_2\ yr^{-1}$	Technical potential; estimates also consider environmental and social factors.	Median and range calculated based on technical and sustainable potentials from Roe et al. (2019).
DACCS	Large	Medium (*low evidence, large agreement*)	5–40 $GtCO_2\ yr^{-1}$	Technical potential	Full range (Fuss et al., 2018).

[a] Potentials classes: low <0.3 $GtCO_2\ yr^{-1}$; moderate 0.3–3 $GtCO_2\ yr^{-1}$; large >3 $GtCO_2\ yr^{-1}$; classification based on *median* potentials estimate.

[b] WGIII will present an update of these estimates based on more recent literature.

5.SM.4 Data Table

Table 5.SM.6 | Input data table. Input datasets and code used to create chapter figures.

Figure Number	Dataset/Code Name	Type	File Name/Specificities	License Type	Dataset/ Code Citation	Dataset/Code URL	Related Publications/ Software Used	Notes
Figure 5.3a	CO_2, 60 Myr BCE. Proxy CO_2 reconstructions based on marine and terrestrial archives.	Input dataset			Chapter 2, AR6		Foster et al. (2017)	
	CO_2, 800 kyr BCE. Ice air-bubble measurement.	Input dataset	Ch2_ice_core.xlsx		Chapter 2, AR6		Bereiter et al. (2015)	
	CO_2, 1–1749 CE. Ice air-bubble measurement.	Input dataset			Chapter 2, AR6		Rubino et al. (2019)	
	CO_2, 1750–2019. Air-bubble and ambient air measurement.	Input dataset	LLGHG_history_AR6_v9_ updated.xlsx		Chapter 2, AR6		Meinshausen et al. (2017)	Updated from Meinshausen et al. (2017) by Jinho Anh
	CO_2, 2020–2100. Model output.	Input dataset						
Figure 5.3b	CO_2, 60 Myr BCE. Proxy CO_2 reconstructions based on marine and terrestrial archives.	Input dataset			Chapter 5, AR6		Python 3.8, for growth rate calculation	
	CO_2, 800 kyr BCE. Ice air-bubble measurement	Input dataset			Chapter 5, AR6		Python 3.8, for growth rate calculation	
	CO_2, 1–1749 year CE. Ice air-bubble measurement.	Input dataset			Chapter 5, AR6		Python 3.8, for growth rate calculation	
	CO_2, 1750–2019. Air-bubble and ambient air measurement.				Chapter 5, AR6		Python 3.8, for growth rate calculation	
	CO_2, 2020–2100. Model output.	Input dataset			Chapter 5, AR6		Python 3.8, for growth rate calculation	
Figure 5.4a	CO_2, 800 kyr BCE. Ice air-bubble measurement.	Input dataset	Ch2_ice_core.xlsx		Chapter 2, AR6		Bereiter et al. (2015); Foster et al. (2017)	
	CO_2, 1–1749 year CE. Ice air-bubble measurement.	Input dataset			Chapter 2, AR6		Rubino et al. (2019)	
	CO_2, 1750–2019. Air-bubble and ambient air measurement.	Input dataset	LLGHG_history_AR6_v9_ updated.xlsx		Chapter 2, AR6		Meinshausen et al. (2017)	Updated from Meinshausen et al. (2017) by Jinho Anh
		Code	AR6_fig5.4_3GHGs_ts.py		Chapter 5, AR6	https://github.com/IPCC-WG1/Chapter-5_Fig04	Python 3.8, for growth rate calculation	
Figure 5.4b	CH_4, 800 kyr BCE. Ice air-bubble measurement.	Input dataset	Ch2_ice_core.xlsx		Chapter 2, AR6		Loulergue et al. (2008)	
	CH_4, 1–1749 year CE. Ice air-bubble measurement.	Input dataset			Chapter 2, AR6		Rubino et al. (2019)	
	CH_4, 1750–2019. Air-bubble and ambient air measurement.	Input dataset	LLGHG_history_AR6_v9_ updated.xlsx		Chapter 2, AR6		Meinshausen et al. (2017)	Updated from Meinshausen et al. (2017) by Jinho Anh
		Code	AR6_fig5.4_3GHGs_ts.py		Chapter 5, AR6	https://github.com/IPCC-WG1/Chapter-5_Fig04	Python 3.8, for growth rate calculation	

Figure Number	Dataset/Code Name	Type	File Name/Specificities	License Type	Dataset/ Code Citation	Dataset/Code URL	Related Publications/ Software Used	Notes
Figure 5.4c	N_2O, 800 kyr BCE. Ice air-bubble measurement.	Input dataset	Ch2_ice_core.xlsx		Chapter 2, AR6		Schilt et al. (2010)	
	N_2O, 1–1749 year CE. Ice air-bubble measurement.	Input dataset			Chapter 2, AR6		Rubino et al. (2019)	
	N_2O, 1750–2019. Air-bubble and ambient air measurement.	Input dataset	LLGHG_history_AR6_v9_updated.xlsx		Chapter 2, AR6		Meinshausen et al. (2017)	Updated from Meinshausen et al. (2017) by Jinho Anh
		Code	AR6_fig5.4_3GHGs_ts.py		Chapter 5, AR6	https://github.com/IPCC-WG1/Chapter-5_Fig04	Python 3.8, for growth rate calculation	
Figure 5.5a	Annual global CO_2 (land-use) emissions. Model-based estimation.	Input dataset					Friedlingstein et al. (2020)	
	Annual global CO_2 (fossil-fuel) emissions. Emission inventory.	Input dataset					Friedlingstein et al. (2020)	
Figure 5.5b	Annual global CO_2 emissions from land-use change. DGVM range.	Input dataset					Friedlingstein et al. (2020)	
	Annual global CO_2 emissions from land-use change. DGVM mean.	Input dataset					Friedlingstein et al. (2020)	
	Annual global CO_2 emissions from land-use change. BLUE.	Input dataset					Hansis et al. (2015)	
	Annual global CO_2 emissions from land-use change. OSCAR.	Input dataset					Gasser et al. (2020)	
	Annual global CO_2 emissions from land-use change. Bookkeeping.	Input dataset					Houghton and Nassikas (2017)	
Figure 5.6a	CO_2, Mauna Loa. Ambient air.	Input dataset	monthly_flask_co2_mlo.csv			Scripps CO_2 Program (http://scrippsco2.ucsd.edu) (accessed 20/05/2022)	Keeling et al. (2001)	SIO/UCSD
	CO_2, South Pole. Ambient air.	Input dataset	monthly_flask_co2_spo.csv			Scripps CO_2 Program (http://scrippsco2.ucsd.edu) (accessed 20/05/2022)	Keeling et al. (2001)	SIO/UCSD
	CO_2, Global, marine background air.	Input dataset	co2_mm_gl.txt				Conway et al. (1994)	GMD/NOAA
	CO_2, GOSAT. Total column dry air mole fractions.	Input dataset	whole-atmosphere-monthly-mean_co2_january_2021.txt			https://www.gosat.nies.go.jp/en/recent-global-co2.html (accessed 20/05/2022)	Yoshida et al. (2013)	NIES
Figure 5.6b	CO_2, Mauna Loa. Ambient air.	Input dataset			Chapter 5, AR6		Nakazawa et al. (1997)	Python 3.8, Nakazawa et al. (1997) for growth rate calculation
	CO_2, South Pole. Ambient air.	Input dataset			Chapter 5, AR6		Nakazawa et al. (1997)	Python 3.8, Nakazawa et al. (1997) for growth rate calculation

Figure Number	Dataset/Code Name	Type	File Name/Specificities	License Type	Dataset/ Code Citation	Dataset/Code URL	Related Publications/ Software Used	Notes
Figure 5.6b *(continued)*	CO_2, Global. Global, marine background air.	Input dataset			Chapter 5, AR6		Nakazawa et al. (1997)	Python 3.8, Nakazawa et al. (1997) for growth rate calculation
	CO_2, GOSAT. Total column dry air mole fractions	Input dataset			Chapter 5, AR6		Nakazawa et al. (1997)	Python 3.8, Nakazawa et al. (1997) for growth rate calculation
Figure 5.6c	d13C-CO_2 Mauna Loa. Ambient air.	Input dataset	monthly_flask_c13_mlo			Scripps CO_2 Program (http://scrippsco2.ucsd.edu) (accessed 20/05/2022)	Keeling et al. (2001)	SIO/UCSD
	d13C-CO_2 South Pole. Ambient air.	Input dataset	monthly_flask_c13_spo			Scripps CO_2 Program (http://scrippsco2.ucsd.edu) (accessed 20/05/2022)	Keeling et al. (2001)	SIO/UCSD
	D14C-CO_2 Wellington. Ambient air.	Input dataset	BHD_14CO2_ datasets_20210309.xlsx				Turnbull et al. (2017)	GNS Science/NIWA
Figure 5.6d	O_2/N_2 Mauna Loa. Ambient air.	Input dataset	mloav.csv			Scripps O_2 Program (http://scrippso2.ucsd.edu) (accessed 20/05/2022)	Keeling and Manning (2014)	SIO/UCSD
	O_2/N_2 South Pole. Ambient air.	Input dataset	spoav.csv			Scripps O_2 Program (http://scrippso2.ucsd.edu) (accessed 20/05/2022)	Keeling and Manning (2014)	SIO/UCSD
Figure 5.7	Anthropogenic emissions, fossil fuel.	Input dataset	Dataset2020_Global_ Budget_v1.0.xlsx				Friedlingstein et al. (2020)	GCP-CO_2
	Anthropogenic emissions, land-use change.	Input dataset	Dataset2020_Global_ Budget_v1.0.xlsx				Friedlingstein et al. (2020)	GCP-CO_2
	CO_2, 1750–2019. Ambient air measurement.	Input dataset	LLGHG_history_AR6_v9_ updated.xlsx		Chapter 2, AR6		Meinshausen et al. (2017)	Updated from Meinshausen et al. (2017) by Jinho Anh
	ENSO Index	Input dataset	meiv2.data				Wolter and Timlin (2011)	
Figure 5.8b	CESM-ETH. Global ocean biogeochemistry model output.	Input dataset	Global_Carbon_ Budget_2020v1.0.xlsx		Friedlingstein et al. (2020)	https://www.icos-cp.eu/science-and-impact/global-carbon-budget/2020 (accessed 20/05/2022)	Doney et al. (2009b)	
	CSIRO. Global ocean biogeochemistry model output.	Input dataset	Global_Carbon_ Budget_2020v1.0.xlsx		Friedlingstein et al. (2020)	https://www.icos-cp.eu/science-and-impact/global-carbon-budget/2020 (accessed 20/05/2022)	Law et al. (2017)	
	FESOM-1.4-REcoM2. Global ocean biogeochemistry model output.	Input dataset	Global_Carbon_ Budget_2020v1.0.xlsx		Friedlingstein et al. (2020)	https://www.icos-cp.eu/science-and-impact/global-carbon-budget/2020 (accessed 20/05/2022)	Hauck et al. (2020)	

Figure Number	Dataset/Code Name	Type	File Name/Specificities	License Type	Dataset/ Code Citation	Dataset/Code URL	Related Publications/ Software Used	Notes
Figure 5.8b *(continued)*	MPIOM-HAMOCC6. Global ocean biogeochemistry model output.	Input dataset	Global_Carbon_ Budget_2020v1.0.xlsx		Friedlingstein et al. (2020)	https://www.icos-cp.eu/science-and-impact/global-carbon-budget/2020 (accessed 20/05/2022)	Paulsen et al. (2017)	
	NEMO3.6-PISCESv2-gas (CNRM). Global ocean biogeochemistry model output.	Input dataset	Global_Carbon_ Budget_2020v1.0.xlsx		Friedlingstein et al. (2020)	https://www.icos-cp.eu/science-and-impact/global-carbon-budget/2020 (accessed 20/05/2022)	Berthet et al. (2019)	
	NEMO-PlankTOM5. Global ocean biogeochemistry model output.	Input dataset	Global_Carbon_ Budget_2020v1.0.xlsx		Friedlingstein et al. (2020)	https://www.icos-cp.eu/science-and-impact/global-carbon-budget/2020 (accessed 20/05/2022)	Buitenhuis et al. (2013)	
	MICOM-HAMOCC (NorESM-OCv1.2). Global ocean biogeochemistry model output.	Input dataset	Global_Carbon_ Budget_2020v1.0.xlsx		Friedlingstein et al. (2020)	https://www.icos-cp.eu/science-and-impact/global-carbon-budget/2020 (accessed 20/05/2022)	Schwinger et al. (2016)	
	MOM6-COBALT (Princeton). Global ocean biogeochemistry model output.	Input dataset	Global_Carbon_ Budget_2020v1.0.xlsx		Friedlingstein et al. (2020)	https://www.icos-cp.eu/science-and-impact/global-carbon-budget/2020 (accessed 20/05/2022)	Liao et al. (2020)	
	NEMO-PISCES (IPSL). Global ocean biogeochemistry model output.	Input dataset	Global_Carbon_ Budget_2020v1.0.xlsx		Friedlingstein et al. (2020)	https://www.icos-cp.eu/science-and-impact/global-carbon-budget/2020 (accessed 20/05/2022)	Aumont et al. (2015)	
	MPI_SOMFFN. Observation-based data product.	Input dataset	ipcc_socom_flux_ annual_20191206.csv				Landschützer et al. (2014)	
	JENA_MLS. Observation-based data product.	Input dataset	ipcc_socom_flux_ annual_20191206.csv				Rödenbeck et al. (2014)	
	LSCE_FFNN2. Observation-based data product.	Input dataset	ipcc_socom_flux_ annual_20191206.csv				Denvil-Sommer et al. (2019)	
	CSIR_ML6. Observation-based data product.	Input dataset	ipcc_socom_flux_ annual_20191206.csv				Gregor et al. (2019)	
	NIES_NN. Observation-based data product.	Input dataset	ipcc_socom_flux_ annual_20191206.csv				Zeng et al. (2014)	
	JMA MLR. Observation-based data product.	Input dataset	ipcc_socom_flux_ annual_20191206.csv				Iida et al. (2020)	
	MIROC4-lr2020. Data of atmospheric CO_2 inversion.	Input dataset					Saeki and Patra (2017)	
	MIROC4-gcp2020. Data of atmospheric CO_2 inversion.	Input dataset					Saeki and Patra (2017)	

Figure Number	Dataset/Code Name	Type	File Name/Specificities	License Type	Dataset/ Code Citation	Dataset/Code URL	Related Publications/ Software Used	Notes
Figure 5.8b *(continued)*	CAMS2020. Data of atmospheric CO_2 inversion.	Input dataset					Chevallier et al. (2005)	
	CTE2020. Data of atmospheric CO_2 inversion.	Input dataset					van der Laan-Luijkx et al. (2017)	
	The oceanic sink for anthropogenic CO_2 from 1994 to 2007 – the data (NCEI Accession 0186034).	Input dataset	inv_dcant_emlr_cstar_ gruber_94-07_vs1.nc		Gruber et al. (2019c)	https://www.ncei.noaa.gov/access/ocean-carbon-data-system/oceans/ndp_100/ndp100.html (accessed 20/05/2022)	Gruber et al. (2019c)	Observation-based data product
	Global decadal variability of the oceanic CO_2 sink. Data of global ocean inverse model.	Input dataset			DeVries et al. (2017)		DeVries et al. (2017)	
	Global carbon budget based on trends in dAPO from three stations in the Scripps O_2 network. Data of global carbon budget from atmospheric O_2/N_2 and CO_2 measurements.	Input dataset			Keeling and Manning (2014)		Keeling and Manning (2014)	
	Global carbon budgets estimated from APO variations in the western Pacific region. Data of global carbon budget from atmospheric O_2/N_2 and CO_2 measurements.	Input dataset			Tohjima et al. (2019)		Tohjima et al. (2019)	
Figure 5.9a	pCO_2 observation-based sea-air CO_2 flux products. Sea-air CO_2 exchange.	Input dataset	FCO2DatProd_mean.nc			https://zenodo.org/record/5482547#.YrLSx9869PY	Landschützer et al. (2014); Rödenbeck et al. (2014); Zeng et al. (2014); Bakker et al. (2016); Denvil-Sommer et al. (2019); Gregor et al. (2019); Iida et al. (2020)	Sea-air CO_2 flux synthesis
Figure 5.b	Anthropogenic CO_2 inventory. Ocean CO_2.	Input dataset	inv_dcant_emlr_cstar_ gruber_94-07_vs1.nc				Gruber et al. (2019c)	
Figure 5.10a	Global net land CO_2 sink. Data derived from global carbon budget.	Input dataset	Global_Carbon_ Budget_2020v1.0.xlsx		Friedlingstein et al. (2020)		Friedlingstein et al. (2020)	
	CarbonTracker-Europe. Atmospheric CO_2 inversion.	Input dataset			van der Laan-Luijkx et al. (2017)		van der Laan-Luijkx et al. (2017)	
	Jena CarboScope. Atmospheric CO_2 inversion.	Input dataset			Rödenbeck et al. (2018)		Rödenbeck et al. (2018)	
	Copernicus Atmosphere Monitoring Service (CAMS). Atmospheric CO_2 inversion.	Input dataset			Chevallier et al. (2005)		Chevallier et al. (2005)	
	MIROC4-ACTM. Atmospheric CO_2 inversion.	Input dataset			Patra et al. (2018)		Patra et al. (2018)	

Figure Number	Dataset/Code Name	Type	File Name/Specificities	License Type	Dataset/ Code Citation	Dataset/Code URL	Related Publications/ Software Used	Notes
Figure 5.10b	AVHRR NDVI. Satellite data.	Input dataset			Tucker et al. (2005)		Tucker et al. (2005)	
	MODIS NDVI. Satellite data.	Input dataset			Didan (2015)	https://doi.org/10.5067/MODIS/MOD13C2.006 (accessed 20/05/2022)		
Figure 5.10c	NIRv. Satellite data.	Input dataset			Badgley et al. (2017)		Badgley et al. (2017)	
	CSIF. Satellite data.	Input dataset			Zhang et al. (2018a)		Zhang et al. (2018a)	
Figure 5.10d	WEC GPP. Data-driven GPP product.	Input dataset			Cheng et al. (2017)		Cheng et al. (2017)	
	MODIS GPP. Satellite-based GPP product	Input dataset			Running and Zhao (2019)	https://lpdaac.usgs.gov/products/mod17a3hgfv006/ (accessed 20/05/2022)		
Figure 5.11	CarbonTracker-Europe. Atmospheric CO_2 inversion.	Input dataset			van der Laan-Luijkx et al.,2017		van der Laan-Luijkx et al. (2017)	
	Jena CarboScope. Atmospheric CO_2 inversion.	Input dataset			Rödenbeck et al., 2018		Rödenbeck et al. (2018)	
	Copernicus Atmosphere Monitoring Service (CAMS). Atmospheric CO_2 inversion.	Input dataset			Chevallier et al., 2005		Chevallier et al. (2005)	
	MIROC4-ACTM. Atmospheric CO_2 inversion.	Input dataset			Patra et al., 2018		Patra et al. (2018)	
	Nino 3.4 index. Sea surface temperature reanalysis.	Input dataset			Rayner (2003)		Rayner (2003)	
	CRU. Gridded temperature observation.	Input dataset			Harris et al. (2014)		Harris et al. (2014)	
Figure 5.13a	CH_4, global. NOAA: global.	Input dataset					Dlugokencky et al. (2003)	
	CH_4, global. AGAGE: global.	Input dataset					Prinn et al. (2018)	
	XCH_4, GOSAT. NIES: GOSAT; total column dry air mole fractions.	Input dataset	whole-atmosphere-monthly-mean_ch4_january_2021.txt			https://www.gosat.nies.go.jp/en/recent-global-ch4.html (accessed 20/05/2022)	Yoshida et al. (2013)	
	CH_4, CMO-THD. PDX: CMO-THD.	Input dataset					Rice et al. (2016)	
	CH_4, CGO. AGAGE: CGO.	Input dataset					Prinn et al. (2018)	
Figure 5.13b	CH_4, global XCH_4, GOSAT CH_4, CMO-THD CH_4, CGO.	Input dataset			Chapter 5, AR6		Python 3.8, Nakazawa et al. (1997) for growth rate calculation	

Figure Number	Dataset/Code Name	Type	File Name/Specificities	License Type	Dataset/ Code Citation	Dataset/Code URL	Related Publications/ Software Used	Notes
Figure 5.13c	d13C-CH_4, NOAA.	Input dataset			White et al. (2018)	ftp://aftp.cmdl.noaa.gov/data/trace_gases/ch4c13/flask/ (accessed 20/05/2022)		
	d13C-CH_4, PDX. PDX: CMO-THD.	Input dataset					Rice et al. (2016)	
Cross-Chapter Box 5.1, Figure 1	CH4, sources/sinks. GCP-CH4.	Input dataset					Kirschke et al. (2013)	
	CH4, sources/sinks. GCP-CH4.	Input dataset	AR6 WGI, Table 5.2				Saunois et al. (2020)	
	CH4, concentration. NOAA: Global.	Input dataset					Dlugokencky et al. (2003)	
Cross-Chapter Box 5.1, Figure 2	LMDz. CH_4 inversion.	Input dataset					Bousquet et al. (2006)	
	TM5-4DVAR. CH_4 inversion.	Input dataset					Bergamaschi et al. (2013)	
	CTE-CH4. CH_4 inversion.	Input dataset					Tsuruta et al. (2017)	
	MIROC4-ACTM. CH_4 inversion.	Input dataset					Chandra et al. (2021)	
	LMDzPyVAR. CH_4 inversion.	Input dataset					Yin et al. (2015)	
	NICAM-TM. CH_4 inversion.	Input dataset					Niwa et al. (2017)	
	NIES-TM-Flexpart. CH_4 inversion.	Input dataset					F. Wang et al. (2019)	
	NIES-TM-GELCA. CH_4 inversion.	Input dataset					Ishizawa et al. (2016)	
	TOMCAT. CH_4 inversion.	Input dataset					McNorton et al. (2018)	
	GCP-WETLAND mean. Land ecosystem model.	Input dataset					Saunois et al. (2020)	
Figure 5.15a	NOAA atmospheric N_2O network dataset	Input dataset	n2o_gbl_mean_grate_noaa.txt		Elkins et al. (2018)	https://www.esrl.noaa.gov/gmd/dv/data/ (accessed 20/05/2022)		https://www.esrl.noaa.gov/gmd/hats/combined/N2O.html
	AGAGE atmospheric N_2O network dataset.	Input dataset	n2o_gbl_mean_grate_agage.txt			https://agage2.eas.gatech.edu/data_archive/agage/ (accessed 20/05/2022)	Prinn et al. (2018)	
	CSIRO atmospheric N_2O network dataset.	Input dataset	n2o_gbl_mean_grate_csiro.txt			https://gaw.kishou.go.jp/ (accessed 20/05/2022)	Francey et al. (2003)	
	Archived air samples from Cape Grim.	Input dataset	N2O_isotope_CGAA_Park_2012.csv				Park et al. (2012)	
	Firn air data set Law Dome.	Input dataset	N2O_isotope_LD_Park_2012.csv				Park et al. (2012)	
	Firn air data set NGRIP.	Input dataset	N2O_isotope_NGRIP_Ishijima_2007.csv			https://ads.nipr.ac.jp/data/search/list/1 (accessed 20/05/2022)	Ishijima et al. (2007)	

Figure Number	Dataset/Code Name	Type	File Name/Specificities	License Type	Dataset/ Code Citation	Dataset/Code URL	Related Publications/ Software Used	Notes
Figure 5.15a *(continued)*	Firn air data set H72.	Input dataset	N2O_isotope_H72_ Ishijima_2007.csv			https://ads.nipr.ac.jp/data/search/list/1 (accessed 20/05/2022)	Ishijima et al. (2007)	
	Firn ice data set Greenland.	Input dataset	N2O_isotope_BRK_ Prokopiou.csv				Prokopiou et al. (2017)	
	Firn ice data set Greenland.	Input dataset	N2O_isotope_DC_ Prokopiou.csv				Prokopiou et al. (2017)	
	Firn ice data set Greenland.	Input dataset	N2O_isotope_DML_ Prokopiou.csv				Prokopiou et al. (2017)	
	Firn ice data set Greenland.	Input dataset	N2O_isotope_NGR_SB_ Prokopiou.csv				Prokopiou et al. (2017)	
	Firn ice data set Greenland.	Input dataset	N2O_isotope_NEEM_09_ Prokopiou.csv				Prokopiou et al. (2017)	
	Firn ice data set Greenland.	Input dataset	N2O_isotope_NEEM_EU_ Prokopiou.csv				Prokopiou et al. (2017)	
	Multivariate ENSO Index.	Input dataset	noaa_mei_ index_1979_2020.txt			https://psl.noaa.gov/enso/mei (accessed 20/05/2022)	Wolter and Timlin (1998)	
Figure 5.15b	Archived air samples from Cape Grim.	Input dataset	N2O_isotope_CGAA_ Park_2012.csv				Park et al. (2012)	
	Firn air data set Law Dome.	Input dataset	N2O_isotope_LD_ Park_2012.csv				Park et al. (2012)	
	Firn air data set NGRIP.	Input dataset	N2O_isotope_NGRIP_ Ishijima_2007.csv				Ishijima et al. (2007)	
	Firn air data set H72.	Input dataset	N2O_isotope_H72_ Ishijima_2007.csv				Ishijima et al. (2007)	
	Firn ice data set Greenland.	Input dataset	N2O_isotope_BRK_ Prokopiou.csv				Prokopiou et al. (2017)	
	Firn ice data set Greenland.	Input dataset	N2O_isotope_DC_ Prokopiou.csv				Prokopiou et al. (2017)	
	Firn ice data set Greenland.	Input dataset	N2O_isotope_DML_ Prokopiou.csv				Prokopiou et al. (2017)	
	Firn ice data set Greenland.	Input dataset	N2O_isotope_NGR_SB_ Prokopiou.csv				Prokopiou et al. (2017)	
	Firn ice data set Greenland.	Input dataset	N2O_isotope_NEEM_09_ Prokopiou.csv				Prokopiou et al. (2017)	
	Firn ice data set Greenland.	Input dataset	N2O_isotope_NEEM_EU_ Prokopiou.csv				Prokopiou et al. (2017)	

Figure Number	Dataset/Code Name	Type	File Name/Specificities	License Type	Dataset/ Code Citation	Dataset/Code URL	Related Publications/ Software Used	Notes
Figure 5.15c	Archived air samples from Cape Grim.	Input dataset	N2O_isotope_CGAA_ Park_2012.csv				Park et al. (2012)	
	Firn air data set H72.	Input dataset	N2O_isotope_H72_ Ishijima_2007.csv				Ishijima et al. (2007)	
	Firn ice data set Greenland.	Input dataset	N2O_isotope_BRK_ Prokopiou.csv				Prokopiou et al. (2017)	
	Firn ice data set Greenland.	Input dataset	N2O_isotope_DC_ Prokopiou.csv				Prokopiou et al. (2017)	
	Firn ice data set. Greenland.	Input dataset	N2O_isotope_DML_ Prokopiou.csv				Prokopiou et al. (2017)	
	Firn ice data set Greenland.	Input dataset	N2O_isotope_NGR_SB_ Prokopiou.csv				Prokopiou et al. (2017)	
	Firn ice data set Greenland.	Input dataset	N2O_isotope_NEEM_09_ Prokopiou.csv				Prokopiou et al. (2017)	
	Firn ice data set Greenland.	Input dataset	N2O_isotope_NEEM_EU_ Prokopiou.csv				Prokopiou et al. (2017)	
Figure 5.17a	Land mean N_2O flux (2007–2016 average). Model simulation.	Input dataset	N2O_emission_density_ IPCC_0716.txt	IPCC data agreement available			Tian et al. (2020)	GCP-N_2O-budget
	Baseline mean and range. Model simulation.	Input dataset	ocean_mean_0716.txt	IPCC data agreement available			Tian et al. (2020)	GCP-N_2O-budget
Figure 5.17 b–p	Total mean and range. Model simulation.	Input dataset	IPCC_NMIP_all_ forcing.xlsx	IPCC data agreement available			Tian et al. (2019)	NMIP
	Baseline mean and range. Model simulation.	Input dataset	IPCC_NMIP_co2_ climate.xlsx	IPCC data agreement available			Tian et al. (2019)	NMIP
Figure 5.18	Effective radiative forcing.	Input dataset	AR6_ERF_all.xlsx		Chapter 7, AR6		Forster, P., et al., Chapter 7, AR6 (2021)	
Figure 5.19	CarbonTracker-Europe. CO_2 inversion.	Input dataset					van der Laan-Luijkx et al. (2017)	GCP-CO_2 Contact: wouter.peters@wur.nl; ingrid.luijkx@wur.nl
	Jena Carboscope. CO_2 inversion.	Input dataset					Rödenbeck et al. (2018)	GCP-CO_2 Contact: Christian.Roedenbeck@bgc-jena.mpg.de
	CAMS. CO_2 inversion.	Input dataset					Chevallier et al. (2005)	GCP-CO_2 Contact: frederic.chevallier@lsce.ipsl.fr
	MIROC4-ACTM. CO_2 inversion.	Input dataset					Patra et al. (2018)	GCP-CO_2 Contact: prabir@jamstec.go.jp; naveennegi@jamstec.go.jp

Figure Number	Dataset/Code Name	Type	File Name/Specificities	License Type	Dataset/ Code Citation	Dataset/Code URL	Related Publications/ Software Used	Notes
Figure 5.19 *(continued)*	NISMON-CO2. CO_2 inversion.	Input dataset					Niwa et al. (2017)	GCP-CO_2 Contact: niwa.yosuke@nies.go.jp
	LMDz. CH_4 inversion.	Input dataset					Bousquet et al. (2006)	GCP-CH_4
	TM5-4DVAR. CH_4 inversion.	Input dataset					Bergamaschi et al. (2013)	GCP-CH_4
	CTE-CH4. CH_4 inversion.	Input dataset					Tsuruta et al. (2017)	GCP-CH_4
	MIROC4-ACTM. CH_4 inversion.	Input dataset					Chandra et al. (2021)	GCP-CH_4
	LMDzPyVAR. CH_4 inversion.	Input dataset					Yin et al. (2015)	GCP-CH_4
	NICAM-TM. CH_4 inversion.	Input dataset					Niwa et al. (2017)	GCP-CH_4
	NIES-TM-Flexpart. CH_4 inversion.	Input dataset					F. Wang et al. (2019)	GCP-CH_4
	NIES-TM-GELCA. CH_4 inversion.	Input dataset					Ishizawa et al. (2016)	GCP-CH_4
	TOMCAT. CH_4 inversion.	Input dataset					McNorton et al. (2018)	GCP-CH_4
	INVICAT. N_2O inversion.	Input dataset					Thompson et al. (2019)	GCP-N_2O Contact: C.Wilson@leeds.ac.uk
	PyVAR-1. N_2O inversion.	Input dataset						GCP-N_2O Contact: rlt@nilu.no
	PyVAR-2. N_2O inversion.	Input dataset						GCP-N_2O Contact: rlt@nilu.no
	MIRO4-ACTM. N_2O inversion.	Input dataset						GCP-N_2O Contact: prabir@jamstec.go.jp
	GEOS-Chem. N_2O inversion.	Input dataset					Tian et al. (2020)	GCP-N_2O Contact: kcw@umn.edu
Figure 5.20	Global surface ocean pH, acidity and Revelle Factor on a 1x1-degree global grid from 1770 to 2100 (NCEI Accession 0206289).	Input dataset	Surface_pH_1770_2000.nc		Jiang et al. (2019)	https://www.ncei.noaa.gov/data/oceans/ncei/ocads/data/0206289/Surface_pH_1770_2100 (accessed 20/05/2022)	Jiang et al. (2019)	Observation-based dataset
	Annual mean seasonally detrended surface ocean pH at time series sites.	Input dataset	annual_mean_pH_seosonally_detrended.xlsx					Observation-based dataset
	Time series data of surface ocean pH at 137E.	Input dataset	137E_surface_carbon.xlsx			https://www.data.jma.go.jp/gmd/kaiyou/db/vessel_obs/data-report/html/ship/ship_e (accessed 20/05/2022)	Ono et al. (2019)	Observation-based dataset

Figure Number	Dataset/Code Name	Type	File Name/Specificities	License Type	Dataset/ Code Citation	Dataset/Code URL	Related Publications/ Software Used	Notes
Figure 5.20 *(continued)*	Time series data of surface ocean pH at stations KNOT and K2.	Input dataset	KNOT_ML.csv, K2_ML.csv			https://www.ncei.noaa.gov/access/ocean-carbon-data-system/oceans/Moorings/K2.html (accessed 20/05/2022)	Wakita et al. (2017)	Observation-based dataset
	Time series data of surface ocean pH at station ALOHA.	Input dataset	HOT_surface_CO2.txt		Dore et al. (2009)	https://hahana.soest.hawaii.edu/hot/products/HOT_surface_CO2.txt (accessed 20/05/2022)	Dore et al. (2009)	Observation-based dataset
	Time series data of surface ocean pH at the BATS site.	Input dataset	43247_2020_30_MOESM2_ESM.xlsx		Bates and Johnson (2020)	https://www.nature.com/articles/s43247-020-00030-5#Sec22 (accessed 20/05/2022)	Bates and Johnson (2020)	Observation-based dataset
	Time series data of surface ocean pH in the Iceland Sea.	Input dataset	IcelandSea.exc.csv, IcelandSea_LN6_2014-2019.csv			https://www.ncei.noaa.gov/access/ocean-carbon-data-system/oceans/Moorings/Iceland_Sea.html (accessed 20/05/2022)	Olafsson et al. (2009)	Observation-based dataset
	Time series data of surface ocean pH at the DYFAMED site.	Input dataset	DYFAMED_surface_pH.csv			https://www.ncei.noaa.gov/access/ocean-carbon-data-system/oceans/Coastal/DYFAMED.html (accessed 20/05/2022)	Merlivat et al. (2018)	Observation-based dataset
	Time series data of surface ocean pH at the ESTOC site.	Input dataset	ESTOC_TS_Data_1995-2016.csv			https://www.ncei.noaa.gov/access/ocean-carbon-data-system/oceans/Coastal/ESTOC.html (accessed 20/05/2022)	González-Dávila et al. (2010)	Observation-based dataset
	Time series data of surface ocean pH at the CARIACO site.	Input dataset	CARIACO_surface_pH.csv			http://imars.marine.usf.edu/CAR-legacy/Master.txt (accessed 20/05/2022)	Bates et al. (2014)	Observation-based dataset
	Time series data of surface ocean pH at the Drake Passage.	Input dataset	DrakePass_pH_Omega_LDEO_030519.PRT.xlsx		Takahashi et al. (2014)	https://www.ldeo.columbia.edu/res/pi/CO2/carbondioxide/pages/pCO2data.html (accessed 20/05/2022)	Takahashi et al. (2014)	Observation-based dataset
	Time series data of surface ocean pH at the Munida site.	Input dataset	MunidaTimeSeries 210106.csv			https://marinedata.niwa.co.nz/nzoa-on-map/ (accessed 20/05/2022)	Bates et al. (2014)	Observation-based dataset

Figure Number	Dataset/Code Name	Type	File Name/Specificities	License Type	Dataset/ Code Citation	Dataset/Code URL	Related Publications/ Software Used	Notes
Figure 5.21	GLODAPv2 mapped data product.	Input dataset	GLODAPv2.2016b_ MappedClimatologies.tar.gz		Lauvset et al. (2016)	https://www.glodap.info/index.php/mapped-data-product/ (accessed 20/05/2022)	Lauvset et al. (2020)	Observation-based dataset
		Input dataset			Olsen et al. (2016)	https://doi.org/10.5194/essd-8-297-2016 (accessed 20/05/2022)		
Figure 5.22_ cmip6	BCC-CSM1-1: historical	Input dataset						
	BCC-CSM2-MR: historical, hist-resIPO	Input dataset			Wu et al. (2018); Zhang et al. (2019)			
	CESM1-BGC: historical	Input dataset						
	CESM2: hist-nat	Input dataset			Danabasoglu (2019c)			
	CESM2_1_001: historical	Input dataset						
	CanESM2: historical	Input dataset						
	CanESM5: historical	Input dataset			Swart et al. (2019c)			
	GFDL-ESM4: historical	Input dataset			Krasting et al. (2018c)			
	HadGEM2-ES: historical	Input dataset						
	IPSL-CM6A-LR: historical	Input dataset			Boucher et al. (2018b)			
	LENS1: historical	Input dataset						
	MIROC-ES2L: historical	Input dataset			Hajima et al. (2019b)			
	MIROC6: historical	Input dataset			Tatebe and Watanabe (2018)			
	NorCPM1: historical	Input dataset			Bethke et al. (2019)			
	NorESM2-LM: historical	Input dataset			Seland et al. (2019)			
	UKESM1-0-LL: historical, piControl	Input dataset			Tang et al. (2019b, c)			
Figure 5.26_ cmip6	ACCESS-ESM1-5: historical, piControl, ssp126, ssp245, ssp370, ssp585	Input dataset			Ziehn et al. (2019c, d, e, f, g, h)			
	CESM2: ssp126, ssp245, ssp370, ssp585	Input dataset			Danabasoglu (2019d, e, f, g)			

Figure Number	Dataset/Code Name	Type	File Name/Specificities	License Type	Dataset/ Code Citation	Dataset/Code URL	Related Publications/ Software Used	Notes
Figure 5.26_ cmip6 *(continued)*	CNRM-ESM2-1: historical, piControl, ssp126, ssp245, ssp370, ssp585	Input dataset			Seferian (2018c, d); Voldoire (2019a, b, c, d)			
	CanESM5: historical, piControl, ssp126, ssp245, ssp370, ssp585	Input dataset			Swart et al. (2019c, d, e, f, g, i)			
	GFDL-ESM4: historical, piControl, ssp126, ssp245, ssp370, ssp585	Input dataset			John et al. (2018a, b, c, d); Krasting et al. (2018c, d)			
	IPSL-CM6A-LR: historical, piControl, ssp126, ssp245, ssp370, ssp585	Input dataset			Boucher et al. (2018b, c, 2019a, b, c, e)			
	MIROC-ES2L: historical, piControl, ssp126, ssp245, ssp370, ssp585	Input dataset			Hajima et al. (2019b, c); Tachiiri et al. (2019a, b, c, d)			
	MPI-ESM1-2-LR: historical, piControl, ssp126, ssp245, ssp370, ssp585	Input dataset			Wieners et al. (2019a, b, c, d, f, g)			
	UKESM1-0-LL: historical, piControl, ssp126, ssp245, ssp370, ssp585	Input dataset			Good et al. (2019a, b, c, e); Tang et al. (2019b, c)			
Figure 5.27_ cmip6	ACCESS-ESM1-5: 1pctCO2-bgc, 1pctCO2, piControl	Input dataset			Ziehn et al. (2019a, b, d)			
	CESM2: 1pctCO2-bgc, 1pctCO2	Input dataset			Danabasoglu (2019a, b)			
	CNRM-ESM2-1: 1pctCO2-bgc, 1pctCO2, piControl	Input dataset			Seferian (2018a, b, d)			
	CanESM5: 1pctCO2-bgc, 1pctCO2, piControl	Input dataset			Swart et al. (2019a, b, d)			
	GFDL-ESM4: 1pctCO2-bgc, 1pctCO2, piControl	Input dataset			Krasting et al. (2018a, b, d)			
	IPSL-CM6A-LR: 1pctCO2-bgc, 1pctCO2, piControl	Input dataset			Boucher et al. (2018a, c, d)			
	MIROC-ES2L: 1pctCO2-bgc, 1pctCO2, piControl	Input dataset			Hajima et al. (2019a, c, d)			
	MPI-ESM1-2-LR: 1pctCO2-bgc, 1pctCO2, piControl	Input dataset			Brovkin et al. (2019); Wieners et al. (2019e, g)			

Figure Number	Dataset/Code Name	Type	File Name/Specificities	License Type	Dataset/ Code Citation	Dataset/Code URL	Related Publications/ Software Used	Notes
Figure 5.27_ cmip6 *(continued)*	UKESM1-0-LL: 1pctCO2-bgc, 1pctCO2, piControl	Input dataset			Jones (2019); Tang et al. (2019a, c)			
Figure 5.30_ cmip6	CESM2-WACCM: historical, piControl, ssp126, ssp534-over, ssp585	Input dataset			Danabasoglu (2019h, i, j, k, l)			
	CanESM5: historical, ssp126, ssp534-over, ssp585	Input dataset			Swart et al. (2019c, e, h, i)			
	IPSL-CM6A-LR: historical, ssp126, ssp534-over, ssp585	Input dataset			Boucher et al. (2018b, 2019a, d, e)			
	UKESM1-0-LL: historical, piControl, ssp126, ssp534-over, ssp585	Input dataset			Good et al. (2019a, d, e); Tang et al. (2019b, c)			
Figure 5.31	IPCC-AR6 assessed historical GSAT time series (Chapter 2).	Input dataset						
	Global Carbon Budget 2020.	Input dataset	2020_Global_Budget_v1.0.xlsx		GCP (2020)	https://doi.org/10.18160/gcp-2020 (accessed 20/05/2022)	Friedlingstein et al. (2020)	
Figure 5.33_ cmip6	CESM2-WACCM: historical, ssp126	Input dataset			Danabasoglu (2019h, j)			
	CanESM5: historical, ssp126	Input dataset			Swart et al. (2019c, e)			
	IPSL-CM6A-LR: historical, ssp126	Input dataset			Boucher et al. (2018b, 2019a)			
	UKESM1-0-LL: historical, ssp126	Input dataset			Good et al. (2019a); Tang et al. (2019b)			
FAQ 5.1	Global Carbon Budget 2020.	Input dataset	2020_Global_Budget_v1.0.xlsx		GCP (2020)	https://doi.org/10.18160/gcp-2020 (accessed 20/05/2022)	Friedlingstein et al. (2020)	
FAQ 5.2	Northern Circumpolar Soil Carbon Database version 2 (NCSCDv2).	Input dataset			Hugelius et al. (2013)	https://bolin.su.se/data/ncscd/ (accessed 20/05/2022)		
	Circumpolar Thermokarst Landscapes Database.	Input dataset			Olefeldt et al. (2016)			

References

Atlas, R. et al., 2011: A Cross-calibrated, Multiplatform Ocean Surface Wind Velocity Product for Meteorological and Oceanographic Applications. *Bulletin of the American Meteorological Society*, **92(2)**, 157–174, doi:10.1175/2010bams2946.1.

Aumont, O., C. Ethé, A. Tagliabue, L. Bopp, and M. Gehlen, 2015: PISCES-v2: an ocean biogeochemical model for carbon and ecosystem studies. *Geoscientific Model Development*, **8(8)**, 2465–2513, doi:10.5194/gmd-8-2465-2015.

Badgley, G., C.B. Field, and J.A. Berry, 2017: Canopy near-infrared reflectance and terrestrial photosynthesis. *Science Advances*, **3(3)**, doi:10.1126/sciadv.1602244.

Bakker, D.C.E. et al., 2016: A multi-decade record of high-quality fCO_2 data in version 3 of the Surface Ocean CO2 Atlas (SOCAT). *Earth System Science Data*, **8(2)**, 383–413, doi:10.5194/essd-8-383-2016.

Bates, N.R. and R.J. Johnson, 2020: Acceleration of ocean warming, salinification, deoxygenation and acidification in the surface subtropical North Atlantic Ocean. *Communications Earth & Environment*, **1(1)**, 33, doi:10.1038/s43247-020-00030-5.

Bates, N.R. et al., 2014: A Time-Series View of Changing Ocean Chemistry Due to Ocean Uptake of Anthropogenic CO_2 and Ocean Acidification. *Oceanography*, **27(1)**, 126–141, doi:10.5670/oceanog.2014.16.

Battle, M. et al., 2000: Global Carbon Sinks and Their Variability Inferred from Atmospheric O2 and δ13C. *Science*, **287(5462)**, 2467–2470, doi:10.1126/science.287.5462.2467.

Bauman, S. et al., 2014: Augmenting the Biological Pump: The Shortcomings of Geoengineered Upwelling. *Oceanography*, **27(3)**, 17–23, doi:10.5670/oceanog.2014.79.

Beerling, D.J. et al., 2018: Farming with crops and rocks to address global climate, food and soil security. *Nature Plants*, **4(3)**, 138–147, doi:10.1038/s41477-018-0108-y.

Benanti, G., M. Saunders, B. Tobin, and B. Osborne, 2014: Contrasting impacts of afforestation on nitrous oxide and methane emissions. *Agricultural and Forest Meteorology*, **198–199**, 82–93, doi:10.1016/j.agrformet.2014.07.014.

Bender, M.L. et al., 2005: Atmospheric O2/N2 changes, 1993–2002: Implications for the partitioning of fossil fuel CO_2 sequestration. *Global Biogeochemical Cycles*, **19(4)**, doi:10.1029/2004gb002410.

Bereiter, B. et al., 2015: Revision of the EPICA Dome C CO_2 record from 800 to 600-kyr before present. *Geophysical Research Letters*, **42(2)**, 542–549, doi:10.1002/2014gl061957.

Bergamaschi, P. et al., 2013: Atmospheric CH 4 in the first decade of the 21st century: Inverse modeling analysis using SCIAMACHY satellite retrievals and NOAA surface measurements. *Journal of Geophysical Research: Atmospheres*, **118(13)**, 7350–7369, doi:10.1002/jgrd.50480.

Berthet, S. et al., 2019: Evaluation of an Online Grid-Coarsening Algorithm in a Global Eddy-Admitting Ocean Biogeochemical Model. *Journal of Advances in Modeling Earth Systems*, **11(6)**, 1759–1783, doi:10.1029/2019ms001644.

Bethke, I. et al., 2019: NCC NorCPM1 model output prepared for CMIP6 CMIP historical. Earth System Grid Federation, doi:10.22033/esgf/cmip6.10894.

Bindoff, N.L. et al., 2019: Changing Ocean, Marine Ecosystems, and Dependent Communities. In: *IPCC Special Report on the Ocean and Cryosphere in a Changing Climate* [Pörtner, H.-O., D.C. Roberts, V. Masson-Delmotte, P. Zhai, M. Tignor, E. Poloczanska, K. Mintenbeck, A. Alegría, M. Nicolai, A. Okem, J. Petzold, B. Rama, and N.M. Weyer (eds.)]. In Press, pp. 447–588, doi:www.ipcc.ch/srocc/chapter/chapter-5.

Blanc-Betes, E. et al., 2020: In silico assessment of the potential of basalt amendments to reduce N2O emissions from bioenergy crops. *GCB Bioenergy*, **13(1)**, 224–241, doi:10.1111/gcbb.12757.

Bock, M. et al., 2017: Glacial/interglacial wetland, biomass burning, and geologic methane emissions constrained by dual stable isotopic CH 4 ice core records. *Proceedings of the National Academy of Sciences*, **114(29)**, E5778–E5786, doi:10.1073/pnas.1613883114.

Boucher, O. et al., 2018a: IPSL IPSL-CM6A-LR model output prepared for CMIP6 CMIP 1pctCO_2. Earth System Grid Federation, doi:10.22033/esgf/cmip6.5049.

Boucher, O. et al., 2018b: IPSL IPSL-CM6A-LR model output prepared for CMIP6 CMIP historical. Earth System Grid Federation, doi:10.22033/esgf/cmip6.5195.

Boucher, O. et al., 2018c: IPSL IPSL-CM6A-LR model output prepared for CMIP6 CMIP piControl. Earth System Grid Federation, doi:10.22033/esgf/cmip6.5251.

Boucher, O. et al., 2018d: IPSL IPSL-CM6A-LR model output prepared for CMIP6 C4MIP 1pctCO_2-bgc. Earth System Grid Federation, doi:10.22033/esgf/cmip6.5050.

Boucher, O. et al., 2019a: IPSL IPSL-CM6A-LR model output prepared for CMIP6 ScenarioMIP ssp126. Earth System Grid Federation, doi:10.22033/esgf/cmip6.5262.

Boucher, O. et al., 2019b: IPSL IPSL-CM6A-LR model output prepared for CMIP6 ScenarioMIP ssp245. Earth System Grid Federation, doi:10.22033/esgf/cmip6.5264.

Boucher, O. et al., 2019c: IPSL IPSL-CM6A-LR model output prepared for CMIP6 ScenarioMIP ssp370. Earth System Grid Federation, doi:10.22033/esgf/cmip6.5265.

Boucher, O. et al., 2019d: IPSL IPSL-CM6A-LR model output prepared for CMIP6 ScenarioMIP ssp534-over. Earth System Grid Federation, doi:10.22033/esgf/cmip6.5269.

Boucher, O. et al., 2019e: IPSL IPSL-CM6A-LR model output prepared for CMIP6 ScenarioMIP ssp585. Earth System Grid Federation, doi:10.22033/esgf/cmip6.5271.

Bousquet, P. et al., 2006: Contribution of anthropogenic and natural sources to atmospheric methane variability. *Nature*, **443(7110)**, 439–443, doi:10.1038/nature05132.

Boyd, P.W. et al., 2007: Mesoscale Iron Enrichment Experiments 1993-2005: Synthesis and Future Directions. *Science*, **315(5812)**, 612–617, doi:10.1126/science.1131669.

Boysen, L.R., W. Lucht, and D. Gerten, 2017: Trade-offs for food production, nature conservation and climate limit the terrestrial carbon dioxide removal potential. *Global Change Biology*, **23(10)**, 4303–4317, doi:10.1111/gcb.13745.

Brovkin, V. et al., 2019: MPI-M MPI-ESM1.2-LR model output prepared for CMIP6 C4MIP 1pctCO_2-bgc. Earth System Grid Federation, doi:10.22033/esgf/cmip6.6437.

Buitenhuis, E.T., T. Hashioka, and C. Quéré, 2013: Combined constraints on global ocean primary production using observations and models. *Global Biogeochemical Cycles*, **27(3)**, 847–858, doi:10.1002/gbc.20074.

Buss, W. and O. Mašek, 2016: High-VOC biochar-effectiveness of post-treatment measures and potential health risks related to handling and storage. *Environmental Science and Pollution Research*, **23(19)**, 19580–19589, doi:10.1007/s11356-016-7112-4.

Butterworth, B.J. and S.D. Miller, 2016: Air-sea exchange of carbon dioxide in the Southern Ocean and Antarctic marginal ice zone. *Geophysical Research Letters*, **43(13)**, 7223–7230, doi:10.1002/2016gl069581.

Cao, L. and K. Caldeira, 2010: Can ocean iron fertilization mitigate ocean acidification? *Climatic Change*, **99(1–2)**, 303–311, doi:10.1007/s10584-010-9799-4.

Cayuela, M.L. et al., 2014: Biochar's role in mitigating soil nitrous oxide emissions: A review and meta-analysis. *Agriculture, Ecosystems & Environment*, **191**, 5–16, doi:10.1016/j.agee.2013.10.009.

Chandra, N. et al., 2021: Emissions from the Oil and Gas Sectors, Coal Mining and Ruminant Farming Drive Methane Growth over the Past Three Decades. *Journal of the Meteorological Society of Japan. Series II*, **99(2)**, doi:10.2151/jmsj.2021-015.

Chaudhuri, A.H., R.M. Ponte, and A.T. Nguyen, 2014: A Comparison of Atmospheric Reanalysis Products for the Arctic Ocean and Implications for Uncertainties in Air–Sea Fluxes. *Journal of Climate*, **27(14)**, 5411–5421, doi:10.1175/jcli-d-13-00424.1.

Chen, P. et al., 2019: Effects of afforestation on soil CH4 and N2O fluxes in a subtropical karst landscape. *Science of The Total Environment*, 135974, doi:10.1016/j.scitotenv.2019.135974.

Cheng, L. et al., 2017: Recent increases in terrestrial carbon uptake at little cost to the water cycle. *Nature Communications*, **8(1)**, 110, doi:10.1038/s41467-017-00114-5.

Chevallier, F., 2013: On the parallelization of atmospheric inversions of CO_2 surface fluxes within a variational framework. *Geoscientific Model Development*, **6(3)**, 783–790, doi:10.5194/gmd-6-783-2013.

Chevallier, F. et al., 2005: Inferring CO_2 sources and sinks from satellite observations: Method and application to TOVS data. *Journal of Geophysical Research: Atmospheres*, **110(D24)**, D24309, doi:10.1029/2005jd006390.

Ciais, P. et al., 2013: Carbon and Other Biogeochemical Cycles. In: *Climate Change 2013: The Physical Science Basis. Contribution of Working Group I to the Fifth Assessment Report of the Intergovernmental Panel on Climate Change* [Stocker, T.F., D. Qin, G.-K. Plattner, M. Tignor, S.K. Allen, J. Boschung, A. Nauels, Y. Xia, V. Bex, and P.M. Midgley (eds.)]. Cambridge University Press, Cambridge, United Kingdom and New York, NY, USA, pp. 465–570, doi:10.1017/cbo9781107415324.015.

Claustre, H., K.S. Johnson, and Y. Takeshita, 2020: Observing the global ccean with biogeochemical-argo. *Annual Review of Marine Science*, **12(1)**, doi:10.1146/annurev-marine-010419-010956.

Clement, D. and N. Gruber, 2018: The eMLR(C*) method to determine decadal changes in the global ocean storage of anthropogenic CO_2. *Global Biogeochemical Cycles*, **32(4)**, 654–679, doi:10.1002/2017gb005819.

Clough, T., L. Condron, C. Kammann, and C. Müller, 2013: A review of biochar and soil nitrogen dynamics. *Agronomy*, **3(2)**, 275–293, doi:10.3390/agronomy3020275.

Conway, T.J. et al., 1994: Evidence for interannual variability of the carbon cycle from the National Oceanic and Atmospheric Administration/Climate Monitoring and Diagnostics Laboratory Global Air Sampling Network. *Journal of Geophysical Research: Atmospheres*, **99(D11)**, 22831, doi:10.1029/94jd01951.

Creutzig, F. et al., 2019: The mutual dependence of negative emission technologies and energy systems. *Energy & Environmental Science*, **12(6)**, 1805–1817, doi:10.1039/c8ee03682a.

Danabasoglu, G., 2019a: NCAR CESM2 model output prepared for CMIP6 C4MIP 1pctCO_2-bgc. Earth System Grid Federation, doi:10.22033/esgf/cmip6.7499.

Danabasoglu, G., 2019b: NCAR CESM2 model output prepared for CMIP6 CMIP 1pctCO_2. Earth System Grid Federation, doi:10.22033/esgf/cmip6.7497.

Danabasoglu, G., 2019c: NCAR CESM2 model output prepared for CMIP6 DAMIP hist-nat. Earth System Grid Federation, doi:10.22033/esgf/cmip6.7609.

Danabasoglu, G., 2019d: NCAR CESM2 model output prepared for CMIP6 ScenarioMIP ssp126. Earth System Grid Federation, doi:10.22033/esgf/cmip6.7746.

Danabasoglu, G., 2019e: NCAR CESM2 model output prepared for CMIP6 ScenarioMIP ssp245. Earth System Grid Federation, doi:10.22033/esgf/cmip6.7748.

Danabasoglu, G., 2019f: NCAR CESM2 model output prepared for CMIP6 ScenarioMIP ssp370. Earth System Grid Federation, doi:10.22033/esgf/cmip6.7753.

Danabasoglu, G., 2019g: NCAR CESM2 model output prepared for CMIP6 ScenarioMIP ssp585. Earth System Grid Federation, doi:10.22033/esgf/cmip6.7768.

Danabasoglu, G., 2019h: NCAR CESM2-WACCM model output prepared for CMIP6 CMIP historical. Earth System Grid Federation, doi:10.22033/esgf/cmip6.10071.

Danabasoglu, G., 2019i: NCAR CESM2-WACCM model output prepared for CMIP6 CMIP piControl. Earth System Grid Federation, doi:10.22033/esgf/cmip6.10094.

Danabasoglu, G., 2019j: NCAR CESM2-WACCM model output prepared for CMIP6 ScenarioMIP ssp126. Earth System Grid Federation, doi:10.22033/esgf/cmip6.10100.

Danabasoglu, G., 2019k: NCAR CESM2-WACCM model output prepared for CMIP6 ScenarioMIP ssp534-over. Earth System Grid Federation, doi:10.22033/esgf/cmip6.10114.

Danabasoglu, G., 2019l: NCAR CESM2-WACCM model output prepared for CMIP6 ScenarioMIP ssp585. Earth System Grid Federation, doi:10.22033/esgf/cmip6.10115.

Daneshvar, F. et al., 2017: Evaluating the significance of wetland restoration scenarios on phosphorus removal. *Journal of Environmental Management*, **192**, 184–196, doi:10.1016/j.jenvman.2017.01.059.

Davin, E.L., S.I. Seneviratne, P. Ciais, A. Olioso, and T. Wang, 2014: Preferential cooling of hot extremes from cropland albedo management. *Proceedings of the National Academy of Sciences*, **111(27)**, 9757–9761, doi:10.1073/pnas.1317323111.

Denman, K.L. et al., 2007: Couplings Between Changes in the Climate System and Biogeochemistry. In: *Climate Change 2007: The Physical Science Basis. Contribution of Working Group I to the Fourth Assessment Report of the Intergovernmental Panel on Climate Change* [Solomon, S., D. Qin, M. Manning, Z. Chen, M. Marquis, K.B. Averyt, M. Tignor, and H.L. Miller (eds.)]. Cambridge University Press, Cambridge, United Kingdom and New York, NY, USA, pp. 499–588, www.ipcc.ch/report/ar4/wg1.

Denvil-Sommer, A., M. Gehlen, M. Vrac, and C. Mejia, 2019: LSCE-FFNN-v1: a two-step neural network model for the reconstruction of surface ocean pCO_2 over the global ocean. *Geoscientific Model Development*, **12(5)**, 2091–2105, doi:10.5194/gmd-12-2091-2019.

Devaraju, N., G. Bala, and A. Modak, 2015a: Effects of large-scale deforestation on precipitation in the monsoon regions: Remote versus local effects. *Proceedings of the National Academy of Sciences*, **112(11)**, 3257–3262, doi:10.1073/pnas.1423439112.

Devaraju, N., G. Bala, and R. Nemani, 2015b: Modelling the influence of land-use changes on biophysical and biochemical interactions at regional and global scales. *Plant, Cell & Environment*, **38(9)**, 1931–1946, doi:10.1111/pce.12488.

DeVries, T., M. Holzer, and F. Primeau, 2017: Recent increase in oceanic carbon uptake driven by weaker upper-ocean overturning. *Nature*, **542(7640)**, 215–218, doi:10.1038/nature21068.

Didan, K., 2015: MOD13C2 MODIS/Terra Vegetation Indices Monthly L3 Global 0.05Deg CMG V006 [Data set]. NASA EOSDIS Land Processes DAAC.

Dlugokencky, E.J. and P. Tans, 2020: Trends in atmospheric carbon dioxide. National Oceanic and Atmospheric Administration Earth System Research Laboratory (NOAA/ESRL).

Dlugokencky, E.J. et al., 2003: Atmospheric methane levels off: Temporary pause or a new steady-state? *Geophysical Research Letters*, **30(19)**, 1992, doi:10.1029/2003gl018126.

Don, A. et al., 2012: Land-use change to bioenergy production in Europe: implications for the greenhouse gas balance and soil carbon. *GCB Bioenergy*, **4(4)**, 372–391, doi:10.1111/j.1757-1707.2011.01116.x.

Doney, S.C. et al., 2009a: Mechanisms governing interannual variability in upper-ocean inorganic carbon system and air–sea CO_2 fluxes: Physical climate and atmospheric dust. *Deep Sea Research Part II: Topical Studies in Oceanography*, **56(8–10)**, 640–655, doi:10.1016/j.dsr2.2008.12.006.

Doney, S.C. et al., 2009b: Mechanisms governing interannual variability in upper-ocean inorganic carbon system and air–sea CO_2 fluxes: Physical climate and atmospheric dust. *Deep Sea Research Part II: Topical Studies in Oceanography*, **56(8)**, 640–655, doi:10.1016/j.dsr2.2008.12.006.

Dore, J.E., R. Lukas, D.W. Sadler, M.J. Church, and D.M. Karl, 2009: Physical and biogeochemical modulation of ocean acidification in the central North Pacific. *Proceedings of the National Academy of Sciences*, **106(30)**, 12235–12240, doi:10.1073/pnas.0906044106.

Elkins, J.W. et al., 2018: Combined Nitrous Oxide data from the NOAA/ESRL Global Monitoring Division. National Oceanic and Atmospheric Administration Earth System Research Laboratory (NOAA/ESRL).

Fairaill, C.W., J.E. Hare, J.B. Edson, and W. McGillis, 2000: Parameterization and Micrometeorological Measurement of Air–Sea Gas Transfer. *Boundary-Layer Meteorology*, **96(1–2)**, 63–106, doi:10.1023/a:1002662826020.

Farley, K.A., E.G. Jobbagy, and R.B. Jackson, 2005: Effects of afforestation on water yield: a global synthesis with implications for policy. *Global Change Biology*, **11(10)**, 1565–1576, doi:10.1111/j.1365-2486.2005.01011.x.

Fay, A.R. and G.A. McKinley, 2014: Global open-ocean biomes: mean and temporal variability. *Earth System Science Data*, **6(2)**, 273–284, doi:10.5194/essd-6-273-2014.

Feng, E.Y., W. Koeve, D.P. Keller, and A. Oschlies, 2017: Model-based assessment of the CO_2 sequestration potential of coastal ocean alkalinization. *Earth's Future*, **5(12)**, 1252–1266, doi:10.1002/2017ef000659.

Fischer, B.M.C. et al., 2019: Improving agricultural water use efficiency with biochar – A synthesis of biochar effects on water storage and fluxes across scales. *Science of The Total Environment*, **657**, 853–862, doi:10.1016/j.scitotenv.2018.11.312.

Flecha, S., F.F. Pérez, A. Murata, A. Makaoui, and I.E. Huertas, 2019: Decadal acidification in Atlantic and Mediterranean water masses exchanging at the Strait of Gibraltar. *Scientific Reports*, **9(1)**, 15533, doi:10.1038/s41598-019-52084-x.

Fornara, D.A. et al., 2011: Increases in soil organic carbon sequestration can reduce the global warming potential of long-term liming to permanent grassland. *Global Change Biology*, **17(5)**, 1925–1934, doi:10.1111/j.1365-2486.2010.02328.x.

Forster, P., T. Storelvmo, K. Armour, W. Collins, J.-L. Dufresne, D. Frame, D.J. Lunt, T. Mauritsen, M.D. Palmer, M. Watanabe, M. Wild, and H. Zhang, 2021: The Earth's Energy Budget, Climate Feedbacks, and Climate Sensitivity. In *Climate Change 2021: The Physical Science Basis. Contribution of Working Group I to the Sixth Assessment Report of the Intergovernmental Panel on Climate Change* [Masson-Delmotte, V., P. Zhai, A. Pirani, S.L. Connors, C. Péan, S. Berger, N. Caud, Y. Chen, L. Goldfarb, M.I. Gomis, M. Huang, K. Leitzell, E. Lonnoy, J.B.R. Matthews, T.K. Maycock, T. Waterfield, O. Yelekçi, R. Yu, and B. Zhou (eds.)]. Cambridge University Press, Cambridge, United Kingdom and New York, NY, USA, pp. 923–1054, doi:10.1017/9781009157896.009.

Foster, G.L., D.L. Royer, and D.J. Lunt, 2017: Future climate forcing potentially without precedent in the last 420 million years. *Nature Communications*, **8**, 14845, doi:10.1038/ncomms14845.

Francey, R.J. et al., 2003: The CSIRO (Australia) measurement of greenhouse gases in the global atmosphere. In: *Report of the eleventh WMO/IAEA Meeting of Experts on Carbon Dioxide Concentration and Related Tracer Measurement Techniques* [Toru, S. and S. Kazuto (eds.)]. WMO TD No. 1138, World Meteorological Organization (WMO), Geneva, Switzerland, pp. 97–111.

Friedlingstein, P. et al., 2019: Global Carbon Budget 2019. *Earth System Science Data*, **11(4)**, 1783–1838, doi:10.5194/essd-11-1783-2019.

Friedlingstein, P. et al., 2020: Global Carbon Budget 2020. *Earth System Science Data*, **12(4)**, 3269–3340, doi:10.5194/essd-12-3269-2020.

Fuss, S. et al., 2018: Negative emissions – Part 2: Costs, potentials and side effects. *Environmental Research Letters*, **13(6)**, 063002, doi:10.1088/1748-9326/aabf9f.

Garbe, C.S. et al., 2014: Transfer across the air-sea interface. *Ocean-Atmosphere Interactions of Gases and Particles*, 55–112, doi:10.1007/978-3-642-25643-1_2.

Gasser, T. et al., 2020: Historical CO_2 emissions from land use and land cover change and their uncertainty. *Biogeosciences*, **17(15)**, 4075–4101, doi:10.5194/bg-17-4075-2020.

GCP, 2020: Supplemental data of Global Carbon Budget 2020 (Version 1.0) [Data set]. Global Carbon Project (GCP).

Genesio, L. et al., 2012: Surface albedo following biochar application in durum wheat. *Environmental Research Letters*, **7(1)**, 014025, doi:10.1088/1748-9326/7/1/014025.

Boyd, P.W. and C.M.G. Vivian (eds.), 2019: *High Level Review of a Wide Range of Proposed Marine Geoengineering Techniques*. Rep. Stud. GESAMP No. 98, IMO/FAO/UNESCO-IOC/UNIDO/WMO/IAEA/UN/UN Environment/UNDP/ISA Joint Group of Experts on the Scientific Aspects of Marine Environmental Protection, 144 pp.

Gloor, M. et al., 2003: A first estimate of present and preindustrial air-sea CO_2 flux patterns based on ocean interior carbon measurements and models. *Geophysical Research Letters*, **30(1)**, 10–1–10–4, doi:10.1029/2002gl015594.

González, M.F. and T. Ilyina, 2016: Impacts of artificial ocean alkalinization on the carbon cycle and climate in Earth system simulations. *Geophysical Research Letters*, **43(12)**, 6493–6502, doi:10.1002/2016gl068576.

González, M.F., T. Ilyina, S. Sonntag, and H. Schmidt, 2018: Enhanced rates of regional warming and ocean acidification after termination of large-scale ocean alkalinization. *Geophysical Research Letters*, **45(14)**, 7120–7129, doi:10.1029/2018gl077847.

González-Dávila, M., J.M. Santana-Casiano, M.J. Rueda, and O. Llinás, 2010: The water column distribution of carbonate system variables at the ESTOC site from 1995 to 2004. *Biogeosciences*, **7(10)**, 3067–3081, doi:10.5194/bg-7-3067-2010.

Good, P. et al., 2019a: MOHC UKESM1.0-LL model output prepared for CMIP6 ScenarioMIP ssp126. Earth System Grid Federation, doi:10.22033/esgf/cmip6.6333.

Good, P. et al., 2019b: MOHC UKESM1.0-LL model output prepared for CMIP6 ScenarioMIP ssp245. Earth System Grid Federation, doi:10.22033/esgf/cmip6.6339.

Good, P. et al., 2019c: MOHC UKESM1.0-LL model output prepared for CMIP6 ScenarioMIP ssp370. Earth System Grid Federation, doi:10.22033/esgf/cmip6.6347.

Good, P. et al., 2019d: MOHC UKESM1.0-LL model output prepared for CMIP6 ScenarioMIP ssp534-over. Earth System Grid Federation, doi:10.22033/esgf/cmip6.6397.

Good, P. et al., 2019e: MOHC UKESM1.0-LL model output prepared for CMIP6 ScenarioMIP ssp585. Earth System Grid Federation, doi:10.22033/esgf/cmip6.6405.

Good, S. et al., 2020: The Current Configuration of the OSTIA System for Operational Production of Foundation Sea Surface Temperature and Ice Concentration Analyses. *Remote Sensing*, **12(4)**, 720, doi:10.3390/rs12040720.

Good, S.A., M.J. Martin, and N.A. Rayner, 2013: EN4: Quality controlled ocean temperature and salinity profiles and monthly objective analyses with uncertainty estimates. *Journal of Geophysical Research: Oceans*, **118(12)**, 6704–6716, doi:10.1002/2013jc009067.

Graven, H.D., N. Gruber, R. Key, S. Khatiwala, and X. Giraud, 2012: Changing controls on oceanic radiocarbon: New insights on shallow-to-deep ocean exchange and anthropogenic CO_2 uptake. *Journal of Geophysical Research: Oceans*, **117(C10)**, doi:10.1029/2012jc008074.

Gray, A.R. et al., 2018: Autonomous biogeochemical Ffoats detect significant carbon dioxide outgassing in the high-latitude Southern Ocean. *Geophysical Research Letters*, **45(17)**, 9049–9057, doi:10.1029/2018gl078013.

Gregor, L. and A.R. Fay, 2021: SeaFlux: harmonised sea-air CO_2 fluxes from surface pCO_2 data products using a standardised approach (2021.04.03) [Data set]. Zenodo.

Gregor, L., A.D. Lebehot, S. Kok, and P.M. Scheel Monteiro, 2019: A comparative assessment of the uncertainties of global surface ocean CO_2 estimates using a machine-learning ensemble (CSIR-ML6 version 2019a) – have we hit the wall? *Geoscientific Model Development*, **12(12)**, 5113–5136, doi:10.5194/gmd-12-5113-2019.

Griscom, B.W. et al., 2017: Natural climate solutions. *Proceedings of the National Academy of Sciences*, **114(44)**, 11645–11650, doi:10.1073/pnas.1710465114.

Gruber, N. and C.D. Keeling, 2001: An improved estimate of the isotopic air-sea disequilibrium of CO_2: Implications for the oceanic uptake of anthropogenic CO_2. *Geophysical Research Letters*, **28(3)**, 555–558, doi:10.1029/2000gl011853.

Gruber, N., P. Landschützer, and N.S. Lovenduski, 2019a: The variable Southern Ocean carbon sink. *Annual Review of Marine Science*, **11(1)**, 159–186, doi:10.1146/annurev-marine-121916-063407.

Gruber, N. et al., 2009: Oceanic sources, sinks, and transport of atmospheric CO_2. *Global Biogeochemical Cycles*, **23(1)**, doi:10.1029/2008gb003349.

Gruber, N. et al., 2019b: The oceanic sink for anthropogenic CO_2 from 1994 to 2007. *Science*, **363(6432)**, 1193–1199, doi:10.1126/science.aau5153.

Gu, J. et al., 2017: Trade-off between soil organic carbon sequestration and nitrous oxide emissions from winter wheat-summer maize rotations: Implications of a 25-year fertilization experiment in Northwestern China. *Science of The Total Environment*, **595**, 371–379, doi:10.1016/j.scitotenv.2017.03.280.

Hajima, T. et al., 2019a: MIROC MIROC-ES2L model output prepared for CMIP6 CMIP 1pctCO_2. Earth System Grid Federation, doi:10.22033/esgf/cmip6.5370.

Hajima, T. et al., 2019b: MIROC MIROC-ES2L model output prepared for CMIP6 CMIP historical. Earth System Grid Federation, doi:10.22033/esgf/cmip6.5602.

Hajima, T. et al., 2019c: MIROC MIROC-ES2L model output prepared for CMIP6 CMIP piControl. Earth System Grid Federation, doi:10.22033/esgf/cmip6.5710.

Hajima, T. et al., 2019d: MIROC MIROC-ES2L model output prepared for CMIP6 C4MIP 1pctCO_2-bgc. Earth System Grid Federation, doi:10.22033/esgf/cmip6.5376.

Hansis, E., S.J. Davis, and J. Pongratz, 2015: Relevance of methodological choices for accounting of land use change carbon fluxes. *Global Biogeochemical Cycles*, doi:10.1002/2014gb004997.

Harper, A.B. et al., 2018: Land-use emissions play a critical role in land-based mitigation for Paris climate targets. *Nature Communications*, **9(1)**, 2938, doi:10.1038/s41467-018-05340-z.

Harris, I., P.D. Jones, T.J. Osborn, and D.H. Lister, 2014: Updated high-resolution grids of monthly climatic observations – the CRU TS3.10 Dataset. *International Journal of Climatology*, **34(3)**, 623–642, doi:10.1002/joc.3711.

Hartmann, J. et al., 2013: Enhanced chemical weathering as a geoengineering strategy to reduce atmospheric carbon dioxide, supply nutrients, and mitigate ocean acidification. *Reviews of Geophysics*, **51(2)**, 113–149, doi:10.1002/rog.20004.

Hauck, J., P. Köhler, D. Wolf-Gladrow, and C. Völker, 2016: Iron fertilisation and century-scale effects of open ocean dissolution of olivine in a simulated CO_2 removal experiment. *Environmental Research Letters*, **11(2)**, 024007, doi:10.1088/1748-9326/11/2/024007.

Hauck, J. et al., 2020: Consistency and Challenges in the Ocean Carbon Sink Estimate for the Global Carbon Budget. *Frontiers in Marine Science*, **7**, 852, doi:10.3389/fmars.2020.571720.

Hauri, C. et al., 2015: Two decades of inorganic carbon dynamics along the West Antarctic Peninsula. *Biogeosciences*, **12(22)**, 6761–6779, doi:10.5194/bg-12-6761-2015.

Heck, V., D. Gerten, W. Lucht, and L.R. Boysen, 2016: Is extensive terrestrial carbon dioxide removal a 'green' form of geoengineering? A global modelling study. *Global and Planetary Change*, **137**, 123–130, doi:10.1016/j.gloplacha.2015.12.008.

Heck, V., D. Gerten, W. Lucht, and A. Popp, 2018: Biomass-based negative emissions difficult to reconcile with planetary boundaries. *Nature Climate Change*, **8(2)**, 151–155, doi:10.1038/s41558-017-0064-y.

Helbig, M. et al., 2020: The biophysical climate mitigation potential of boreal peatlands during the growing season. *Environmental Research Letters*, **15(10)**, doi:10.1088/1748-9326/abab34.

Hemes, K.S. et al., 2018: A Unique Combination of Aerodynamic and Surface Properties Contribute to Surface Cooling in Restored Wetlands of the Sacramento-San Joaquin Delta, California. *Journal of Geophysical Research: Biogeosciences*, **123(7)**, 2072–2090, doi:10.1029/2018jg004494.

Hersbach, H. et al., 2020: The ERA5 global reanalysis. *Quarterly Journal of the Royal Meteorological Society*, **146(730)**, 1999–2049, doi:10.1002/qj.3803.

Houghton, R.A. and A.A. Nassikas, 2017: Global and regional fluxes of carbon from land use and land cover change 1850-2015. *Global Biogeochemical Cycles*, **31(3)**, 456–472, doi:10.1002/2016gb005546.

Huang, Y. et al., 2019: Methane and Nitrous Oxide Flux after Biochar Application in Subtropical Acidic Paddy Soils under Tobacco-Rice Rotation. *Scientific Reports*, **9(1)**, 17277, doi:10.1038/s41598-019-53044-1.

Hugelius, G. et al., 2013: A new data set for estimating organic carbon storage to 3 m depth in soils of the northern circumpolar permafrost region. *Earth System Science Data*, **5(2)**, 393–402, doi:10.5194/essd-5-393-2013.

Iida, Y., Y. Takatani, A. Kojima, and M. Ishii, 2020: Global trends of ocean CO_2 sink and ocean acidification: an observation-based reconstruction of surface ocean inorganic carbon variables. *Journal of Oceanography*, **77**, 323–358, doi:10.1007/s10872-020-00571-5.

IPCC, 2019: IPCC Special Report on the Ocean and Cryosphere in a Changing Climate [Pörtner, H.-O., D.C. Roberts, V. Masson-Delmotte, P. Zhai, M. Tignor, E. Poloczanska, K. Mintenbeck, A. Alegría, M. Nicolai, A. Okem, J. Petzold, B. Rama, and N.M. Weyer (eds.)]. In Press, 755 pp., doi:www.ipcc.ch/report/srocc.

Ishii, M. et al., 2011: Ocean acidification off the south coast of Japan: A result from time series observations of CO_2 parameters from 1994 to 2008. *Journal of Geophysical Research: Oceans*, **116(C6)**, C06022, doi:10.1029/2010jc006831.

Ishii, M. et al., 2020: Ocean Acidification From Below in the Tropical Pacific. *Global Biogeochemical Cycles*, **34(8)**, e2019GB006368, doi:10.1029/2019gb006368.

Ishijima, K. et al., 2007: Temporal variations of the atmospheric nitrous oxide concentration and its δ15N and δ18O for the latter half of the 20th century reconstructed from firn air analyses. *Journal of Geophysical Research: Atmospheres*, **112(D3)**, D03305, doi:10.1029/2006jd007208.

Ishizawa, M. et al., 2016: Inter-annual variability of summertime CO 2 exchange in Northern Eurasia inferred from GOSAT XCO 2. *Environmental Research Letters*, **11(10)**, 105001, doi:10.1088/1748-9326/11/10/105001.

Jacobson, A.R., S.E. Mikaloff Fletcher, N. Gruber, J.L. Sarmiento, and M. Gloor, 2007: A joint atmosphere–ocean inversion for surface fluxes of carbon dioxide: 1. Methods and global-scale fluxes. *Global Biogeochemical Cycles*, **21(1)**, GB1019, doi:10.1029/2005gb002556.

Jeffery, S., F.G.A. Verheijen, C. Kammann, and D. Abalos, 2016: Biochar effects on methane emissions from soils: A meta-analysis. *Soil Biology and Biochemistry*, **101**, 251–258, doi:10.1016/j.soilbio.2016.07.021.

Jia, G. et al., 2019: Land–climate interactions. In: *Climate Change and Land: an IPCC special report on climate change, desertification, land degradation, sustainable land management, food security, and greenhouse gas fluxes in terrestrial ecosystems.* [Shukla, P.R., J. Skea, E.C. Buendia, V. Masson-Delmotte, H.-O. Pörtner, D.C. Roberts, P. Zhai, R. Slade, S. Connors, R. Diemen, M. Ferrat, E. Haughey, S. Luz, S. Neogi, M. Pathak, J. Petzold, J.P. Pereira,

P. Vyas, E. Huntley, K. Kissick, M. Belkacemi, and J. Malley (eds.)]. In Press, pp. 131–248, doi:www.ipcc.ch/srccl/chapter/chapter-2.

Jiang, L.-Q., B.R. Carter, R.A. Feely, S.K. Lauvset, and A. Olsen, 2019: Surface ocean pH and buffer capacity: past, present and future. *Scientific Reports*, **9(1)**, 18624, doi:10.1038/s41598-019-55039-4.

Jin, X. and N. Gruber, 2003: Offsetting the radiative benefit of ocean iron fertilization by enhancing N 2 O emissions. *Geophysical Research Letters*, **30(24)**, 2249, doi:10.1029/2003gl018458.

John, J.G. et al., 2018a: NOAA-GFDL GFDL-ESM4 model output prepared for CMIP6 ScenarioMIP ssp126. Earth System Grid Federation, doi:10.22033/esgf/cmip6.8684.

John, J.G. et al., 2018b: NOAA-GFDL GFDL-ESM4 model output prepared for CMIP6 ScenarioMIP ssp245. Earth System Grid Federation, doi:10.22033/esgf/cmip6.8686.

John, J.G. et al., 2018c: NOAA-GFDL GFDL-ESM4 model output prepared for CMIP6 ScenarioMIP ssp370. Earth System Grid Federation, doi:10.22033/esgf/cmip6.8691.

John, J.G. et al., 2018d: NOAA-GFDL GFDL-ESM4 model output prepared for CMIP6 ScenarioMIP ssp585. Earth System Grid Federation, doi:10.22033/esgf/cmip6.8706.

Jones, C., 2019: MOHC UKESM1.0-LL model output prepared for CMIP6 C4MIP 1pctCO_2-bgc. Earth System Grid Federation, doi:10.22033/esgf/cmip6.5796.

Jones, C.D. et al., 2016: Simulating the Earth system response to negative emissions.

Joos, F., R. Meyer, M. Bruno, and M. Leuenberger, 1999: The variability in the carbon sinks as reconstructed for the last 1000 years. *Geophysical Research Letters*, **26(10)**, 1437–1440, doi:10.1029/1999gl900250.

Kammann, C. et al., 2017: Biochar as a Tool to teduce the Agricultural Greenhouse-gas Burden – Knowns, Unknowns and Future Research Needs. *Journal of Environmental Engineering and Landscape Management*, **25(2)**, 114–139, doi:10.3846/16486897.2017.1319375.

Kantola, I.B., M.D. Masters, D.J. Beerling, S.P. Long, and E.H. DeLucia, 2017: Potential of global croplands and bioenergy crops for climate change mitigation through deployment for enhanced weathering. *Biology Letters*, **13(4)**, 20160714, doi:10.1098/rsbl.2016.0714.

Karhu, K., T. Mattila, I. Bergström, and K. Regina, 2011: Biochar addition to agricultural soil increased CH4 uptake and water holding capacity – Results from a short-term pilot field study. *Agriculture, Ecosystems & Environment*, **140(1)**, 309–313, doi:10.1016/j.agee.2010.12.005.

Kaushal, S.S. et al., 2018: Freshwater salinization syndrome on a continental scale. *Proceedings of the National Academy of Sciences*, **115(4)**, E574–E583, doi:10.1073/pnas.1711234115.

Keeling, C.D., T.P. Whorf, M. Wahlen, and J. van der Plicht, 2001: *Exchanges of Atmospheric CO_2 and 13CO_2 with the Terrestrial Biosphere and Oceans from 1978 to 2000. I. Global Aspects*. SIO Reference No. 01–06, Scripps Institution of Oceanography, University of California San Diego, San Diego, CA, USA, 28 pp.

Keeling, R.F. and A.C. Manning, 2014: Studies of Recent Changes in Atmospheric O2 Content. In: *Treatise on Geochemistry (Second Edition)* [Holland, H.D. and K.K. Turekian (eds.)]. Elsevier, pp. 385–404, doi:10.1016/b978-0-08-095975-7.00420-4.

Keller, D.P., E.Y. Feng, and A. Oschlies, 2014: Potential climate engineering effectiveness and side effects during a high carbon dioxide-emission scenario. *Nature Communications*, **5(1)**, 3304, doi:10.1038/ncomms4304.

Keller, D.P. et al., 2018: The Effects of Carbon Dioxide Removal on the Carbon Cycle. *Current Climate Change Reports*, **4(3)**, 250–265, doi:10.1007/s40641-018-0104-3.

Key, R.M. et al., 2004: A global ocean carbon climatology: Results from Global Data Analysis Project (GLODAP). *Global Biogeochemical Cycles*, **18(4)**, GB4031, doi:10.1029/2004gb002247.

Kirschke, S. et al., 2013: Three decades of global methane sources and sinks. *Nature Geoscience*, **6(10)**, 813–823, doi:10.1038/ngeo1955.

Kitidis, V., I. Brown, N. Hardman-Mountford, and N. Lefèvre, 2017: Surface ocean carbon dioxide during the Atlantic Meridional Transect (1995–2013); evidence of ocean acidification. *Progress in Oceanography*, **158**, 65–75, doi:10.1016/j.pocean.2016.08.005.

Kluber, L.A. et al., 2014: Multistate assessment of wetland restoration on CO_2 and N2O emissions and soil bacterial communities. *Applied Soil Ecology*, **76**, 87–94, doi:10.1016/j.apsoil.2013.12.014.

Kobayashi, S. et al., 2015: The JRA-55 Reanalysis: General Specifications and Basic Characteristics. *Journal of the Meteorological Society of Japan. Series II*, **93(1)**, 5–48, doi:10.2151/jmsj.2015-001.

Köhler, P., J.F. Abrams, C. Völker, J. Hauck, and D.A. Wolf-Gladrow, 2013: Geoengineering impact of open ocean dissolution of olivine on atmospheric CO_2, surface ocean pH and marine biology. *Environmental Research Letters*, **8(1)**, 014009, doi:10.1088/1748-9326/8/1/014009.

Koskinen, M. et al., 2017: Restoration of nutrient-rich forestry-drained peatlands poses a risk for high exports of dissolved organic carbon, nitrogen, and phosphorus. *Science of The Total Environment*, **586**, 858–869, doi:10.1016/j.scitotenv.2017.02.065.

Krakauer, N.Y., J.T. Randerson, F.W. Primeau, N. Gruber, and D. Menemenlis, 2006: Carbon isotope evidence for the latitudinal distribution and wind speed dependence of the air–sea gas transfer velocity. *Tellus B: Chemical and Physical Meteorology*, **58(5)**, 390–417, doi:10.1111/j.1600-0889.2006.00223.x.

Krasting, J.P. et al., 2018a: NOAA-GFDL GFDL-ESM4 model output prepared for CMIP6 C4MIP 1pctCO_2-bgc. Earth System Grid Federation, doi:10.22033/esgf/cmip6.8475.

Krasting, J.P. et al., 2018b: NOAA-GFDL GFDL-ESM4 model output prepared for CMIP6 CMIP 1pctCO_2. Earth System Grid Federation, doi:10.22033/esgf/cmip6.8473.

Krasting, J.P. et al., 2018c: NOAA-GFDL GFDL-ESM4 model output prepared for CMIP6 CMIP historical. Earth System Grid Federation, doi:10.22033/esgf/cmip6.8597.

Krasting, J.P. et al., 2018d: NOAA-GFDL GFDL-ESM4 model output prepared for CMIP6 CMIP piControl. Earth System Grid Federation, doi:10.22033/esgf/cmip6.8669.

Krause, A. et al., 2017: Global consequences of afforestation and bioenergy cultivation on ecosystem service indicators. *Biogeosciences*, **14(21)**, 4829–4850, doi:10.5194/bg-14-4829-2017.

Kraxner, F. et al., 2013: Global bioenergy scenarios – Future forest development, land-use implications, and trade-offs. *Biomass and Bioenergy*, **57**, 86–96, doi:10.1016/j.biombioe.2013.02.003.

Kwiatkowski, L., K.L. Ricke, and K. Caldeira, 2015: Atmospheric consequences of disruption of the ocean thermocline. *Environmental Research Letters*, **10(3)**, 034016, doi:10.1088/1748-9326/10/3/034016.

Landschützer, P., N. Gruber, and D.C.E. Bakker, 2016: Decadal variations and trends of the global ocean carbon sink. *Global Biogeochemical Cycles*, **30(10)**, 1396–1417, doi:10.1002/2015gb005359.

Landschützer, P., N. Gruber, and D.C.E. Bakker, 2020: An observation-based global monthly gridded sea surface pCO_2 product from 1982 onward and its monthly climatology (NCEI Accession 0160558). *NOAA National Centers for Environmental Information*, Version 5.5, doi:10.7289/v5z899n6.

Landschützer, P., N. Gruber, D.C.E. Bakker, and U. Schuster, 2014: Recent variability of the global ocean carbon sink. *Global Biogeochemical Cycles*, **28(9)**, 927–949, doi:10.1002/2014gb004853.

Landschützer, P., N. Gruber, D.C.E. Bakker, I. Stemmler, and K.D. Six, 2018: Strengthening seasonal marine CO_2 variations due to increasing atmospheric CO_2. *Nature Climate Change*, **8(2)**, 146–150, doi:10.1038/s41558-017-0057-x.

Laruelle, G.G. et al., 2017: Global high-resolution monthly CO_2 climatology for the coastal ocean derived from neural network interpolation. *Biogeosciences*, **14(19)**, 4545–4561, doi:10.5194/bg-14-4545-2017.

Lauvset, S.K. and N. Gruber, 2014: Long-term trends in surface ocean pH in the North Atlantic. *Marine Chemistry*, **162**, 71–76, doi:10.1016/j.marchem.2014.03.009.

Lauvset, S.K., N. Gruber, P. Landschützer, A. Olsen, and J. Tjiputra, 2015: Trends and drivers in global surface ocean pH over the past 3 decades. *Biogeosciences*, **12(5)**, 1285–1298, doi:10.5194/bg-12-1285-2015.

Lauvset, S.K. et al., 2016: A new global interior ocean mapped climatology: the 1° × 1° GLODAP version 2. *Earth System Science Data*, **8(2)**, 325–340, doi:10.5194/essd-8-325-2016.

Lauvset, S.K. et al., 2020: Processes driving global interior ocean pH distribution. *Global Biogeochemical Cycles*, 2019GB006229, doi:10.1029/2019gb006229.

Law, R.M. et al., 2017: The carbon cycle in the Australian Community Climate and Earth System Simulator (ACCESS-ESM1) – Part 1: Model description and pre-industrial simulation. *Geoscientific Model Development*, **10(7)**, 2567–2590, doi:10.5194/gmd-10-2567-2017.

Liao, E., L. Resplandy, J. Liu, and K.W. Bowman, 2020: Amplification of the Ocean Carbon Sink During El Niños: Role of Poleward Ekman Transport and Influence on Atmospheric CO_2. *Global Biogeochemical Cycles*, **34(9)**, e2020GB006574, doi:10.1029/2020gb006574.

Liu, C. et al., 2016: Biochar increased water holding capacity but accelerated organic carbon leaching from a sloping farmland soil in China. *Environmental Science and Pollution Research*, **23(2)**, 995–1006, doi:10.1007/s11356-015-4885-9.

Liu, Z. et al., 2017: Effects of biochar application on nitrogen leaching, ammonia volatilization and nitrogen use efficiency in two distinct soils. *Journal of soil science and plant nutrition*, **17(2)**, 515–528, doi:10.4067/s0718-95162017005000037.

Loulergue, L. et al., 2008: Orbital and millennial-scale features of atmospheric CH4 over the past 800,000 years. *Nature*, **453(7193)**, 383–386, doi:10.1038/nature06950.

Marcellin Yao, K. et al., 2016: Time variability of the north-western Mediterranean Sea pH over 1995–2011. *Marine Environmental Research*, **116**, 51–60, doi:10.1016/j.marenvres.2016.02.016.

McGillis, W.R., J.B. Edson, J.E. Hare, and C.W. Fairall, 2001: Direct covariance air-sea CO_2 fluxes. *Journal of Geophysical Research: Oceans*, **106(C8)**, 16729–16745, doi:10.1029/2000jc000506.

McKinley, G.A., A.R. Fay, N.S. Lovenduski, and D.J. Pilcher, 2017: Natural Variability and Anthropogenic Trends in the Ocean Carbon Sink. *Annual Review of Marine Science*, **9(1)**, 125–150, doi:10.1146/annurev-marine-010816-060529.

McKinley, G.A., A.R. Fay, Y.A. Eddebbar, L. Gloege, and N.S. Lovenduski, 2020: External Forcing Explains Recent Decadal Variability of the Ocean Carbon Sink. *AGU Advances*, **1(2)**, doi:10.1029/2019av000149.

Mcneil, B.I., R.J. Matear, R.M. Keyjohn, L. Bullisterand, and J.L. Sarmiento, 2003: Anthropogenic CO_2 Uptake by the Ocean Based on the Global Chlorofluorocarbon Data Set. *Science*, **299(5604)**, 235–239, doi:10.1126/science.1077429.

McNorton, J. et al., 2018: Attribution of recent increases in atmospheric methane through 3-D inverse modelling. *Atmospheric Chemistry and Physics*, **18(24)**, 18149–18168, doi:10.5194/acp-18-18149-2018.

Meinshausen, M. et al., 2017: Historical greenhouse gas concentrations for climate modelling (CMIP6). *Geoscientific Model Development*, **10(5)**, 2057–2116, doi:10.5194/gmd-10-2057-2017.

Meli, P., J.M. Rey Benayas, P. Balvanera, and M. Martínez Ramos, 2014: Restoration enhances wetland biodiversity and ecosystem service supply, but results are context-dependent: a meta-analysis. *PloS one*, **9(4)**, e93507–e93507, doi:10.1371/journal.pone.0093507.

Mengis, N., D.P. Keller, W. Rickels, M. Quaas, and A. Oschlies, 2019: Climate engineering–induced changes in correlations between Earth system variables-implications for appropriate indicator selection. *Climatic Change*, **153(3)**, 305–322, doi:10.1007/s10584-019-02389-7.

Merlivat, L. et al., 2018: Increase of dissolved inorganic carbon and decrease in pH in near-surface waters in the Mediterranean Sea during the past two decades. *Biogeosciences*, **15(18)**, 5653–5662, doi:10.5194/bg-15-5653-2018.

Midorikawa, T. et al., 2012: Recent deceleration of oceanic pCO_2 increase in the western North Pacific in winter. *Geophysical Research Letters*, **39(12)**, L12601, doi:10.1029/2012gl051665.

Mikaloff Fletcher, S.E. et al., 2006: Inverse estimates of anthropogenic CO_2 uptake, transport, and storage by the ocean. *Global Biogeochemical Cycles*, **20(2)**, doi:10.1029/2005gb002530.

Molari, M. et al., 2018: CO_2 leakage alters biogeochemical and ecological functions of submarine sands. *Science Advances*, **4(2)**, eaao2040, doi:10.1126/sciadv.aao2040.

Müller, S.A., F. Joos, G.-K. Plattner, N.R. Edwards, and T.F. Stocker, 2008: Modeled natural and excess radiocarbon: Sensitivities to the gas exchange formulation and ocean transport strength. *Global Biogeochemical Cycles*, **22(3)**, n/a–n/a, doi:10.1029/2007gb003065.

Naegler, T., 2009: Reconciliation of excess 14C-constrained global CO_2 piston velocity estimates. *Tellus B: Chemical and Physical Meteorology*, **61(2)**, 372–384, doi:10.1111/j.1600-0889.2008.00408.x.

Nakano, H., M. Ishii, K.B. Rodgers, H. Tsujino, and G. Yamanaka, 2015: Anthropogenic CO_2 uptake, transport, storage, and dynamical controls in the ocean imposed by the meridional overturning circulation: A modeling study. *Global Biogeochemical Cycles*, **29(10)**, 1706–1724, doi:10.1002/2015gb005128.

Nakazawa, T., S. Morimoto, S. Aoki, and M. Tanaka, 1997: Temporal and spatial variations of the carbon isotopic ratio of atmospheric carbon dioxide in the western Pacific region. *Journal of Geophysical Research: Atmospheres*, **102(D1)**, 1271–1285, doi:10.1029/96jd02720.

NASEM, 2019: *Negative Emissions Technologies and Reliable Sequestration: A Research Agenda*. National Academies of Sciences, Engineering, and Medicine (NASEM). The National Academies Press, Washington, DC, USA, 510 pp., doi:10.17226/25259.

Nightingale, P.D. et al., 2000: In situ evaluation of air-sea gas exchange parameterizations using novel conservative and volatile tracers. *Global Biogeochemical Cycles*, **14(1)**, 373–387, doi:10.1029/1999gb900091.

Niwa, Y. et al., 2017: A 4D-Var inversion system based on the icosahedral grid model (NICAM-TM 4D-Var v1.0) – Part 1: Offline forward and adjoint transport models. *Geoscientific Model Development*, **10(3)**, 1157–1174, doi:10.5194/gmd-10-1157-2017.

Olafsson, J. et al., 2009: Rate of Iceland Sea acidification from time series measurements. *Biogeosciences*, **6(11)**, 2661–2668, doi:10.5194/bg-6-2661-2009.

Olefeldt, D. et al., 2016: Arctic Circumpolar Distribution and Soil Carbon of Thermokarst Landscapes, 2015. ORNL Distributed Active Archive Center, Oak Ridge, TN, USA.

Olsen, A. et al., 2016: The Global Ocean Data Analysis Project version 2 (GLODAPv2) – an internally consistent data product for the world ocean. *Earth System Science Data*, **8(2)**, 297–323, doi:10.5194/essd-8-297-2016.

Ono, H. et al., 2019: Acceleration of ocean acidification in the Western North Pacific. *Geophysical Research Letters*, **46(n/a)**, 13161–13169, doi:10.1029/2019gl085121.

Oschlies, A., W. Koeve, W. Rickels, and K. Rehdanz, 2010a: Side effects and accounting aspects of hypothetical large-scale Southern Ocean iron fertilization. *Biogeosciences*, **7(12)**, 4017–4035, doi:10.5194/bg-7-4017-2010.

Oschlies, A., M. Pahlow, A. Yool, and R.J. Matear, 2010b: Climate engineering by artificial ocean upwelling: Channelling the sorcerer's apprentice. *Geophysical Research Letters*, **37(4)**, doi:10.1029/2009gl041961.

Park, S. et al., 2012: Trends and seasonal cycles in the isotopic composition of nitrous oxide since 1940. *Nature Geoscience*, **5(4)**, 261–265, doi:10.1038/ngeo1421.

Patra, P.K. et al., 2018: Improved Chemical Tracer Simulation by MIROC4.0-based Atmospheric Chemistry-Transport Model (MIROC4-ACTM). *SOLA*, **14**, 91–96, doi:10.2151/sola.2018-016.

Paulsen, H., T. Ilyina, K.D. Six, and I. Stemmler, 2017: Incorporating a prognostic representation of marine nitrogen fixers into the global ocean biogeochemical model HAMOCC. *Journal of Advances in Modeling Earth Systems*, **9(1)**, 438–464, doi:10.1002/2016ms000737.

Paustian, K., E. Larson, J. Kent, E. Marx, and A. Swan, 2019: Soil C Sequestration as a Biological Negative Emission Strategy. *Frontiers in Climate*, **1**, 8, doi:10.3389/fclim.2019.00008.

Paustian, K. et al., 2016: Climate-smart soils. *Nature*, **532(7597)**, 49–57, doi:10.1038/nature17174.

Pongratz, J., C.H. Reick, T. Raddatz, and M. Claussen, 2010: Biogeophysical versus biogeochemical climate response to historical anthropogenic land cover change. *Geophysical Research Letters*, **37(8)**, L08702, doi:10.1029/2010gl043010.

Prentice, I.C. et al., 2001: The carbon cycle and atmospheric carbon dioxide. In: *Climate Change 2001: The Scientific Basis. Contribution of Working Group I to the Third Assessment Report of the Intergovernmental Panel on Climate Change* [Houghton, J.T., Y. Ding, D.J. Griggs, M. Noguer, P.J. van der Linden, X. Dai, K. Maskell, and C.A. Johnson (eds.)]. Cambridge University Press, Cambridge, United Kingdom and New York, NY, USA, pp. 183–237, doi:www.ipcc.ch/report/ar3/wg1/.

Prinn, R.G. et al., 2018: History of chemically and radiatively important atmospheric gases from the Advanced Global Atmospheric Gases Experiment (AGAGE). *Earth System Science Data*, **10(2)**, 985–1018, doi:10.5194/essd-10-985-2018.

Prokopiou, M. et al., 2017: Constraining N2O emissions since 1940 using firn air isotope measurements in both hemispheres. *Atmospheric Chemistry and Physics*, **17(7)**, 4539–4564, doi:10.5194/acp-17-4539-2017.

Ramon, J., L. Lledó, V. Torralba, A. Soret, and F.J. Doblas-Reyes, 2019: What global reanalysis best represents near-surface winds? *Quarterly Journal of the Royal Meteorological Society*, **145(724)**, 3236–3251, doi:10.1002/qj.3616.

Rayner, N.A., 2003: Global analyses of sea surface temperature, sea ice, and night marine air temperature since the late nineteenth century. *Journal of Geophysical Research: Atmospheres*, **108(D14)**, 4407, doi:10.1029/2002jd002670.

Renforth, P. and G. Henderson, 2017: Assessing ocean alkalinity for carbon sequestration. *Reviews of Geophysics*, **55(3)**, 636–674, doi:10.1002/2016rg000533.

Resplandy, L. et al., 2018: Revision of global carbon fluxes based on a reassessment of oceanic and riverine carbon transport. *Nature Geoscience*, **11(7)**, 504–509, doi:10.1038/s41561-018-0151-3.

Rice, A.L. et al., 2016: Atmospheric methane isotopic record favors fossil sources flat in 1980s and 1990s with recent increase. *Proceedings of the National Academy of Sciences*, **113(39)**, 10791–10796, doi:10.1073/pnas.1522923113.

Rödenbeck, C., S. Zaehle, R. Keeling, and M. Heimann, 2018: How does the terrestrial carbon exchange respond to inter-annual climatic variations? A quantification based on atmospheric CO_2 data. *Biogeosciences*, **15(8)**, 2481–2498, doi:10.5194/bg-15-2481-2018.

Rödenbeck, C. et al., 2013: Global surface-ocean pCO_2 and sea–air CO_2 flux variability from an observation-driven ocean mixed-layer. *Ocean Science*, **9(2)**, 193–216, doi:10.5194/os-9-193-2013.

Rödenbeck, C. et al., 2014: Interannual sea–air CO_2 flux variability from an observation-driven ocean mixed-layer scheme. *Biogeosciences*, **11(17)**, 4599–4613, doi:10.5194/bg-11-4599-2014.

Rödenbeck, C. et al., 2015: Data-based estimates of the ocean carbon sink variability – first results of the Surface Ocean pCO_2 Mapping intercomparison (SOCOM). *Biogeosciences*, **12(23)**, 7251–7278, doi:10.5194/bg-12-7251-2015.

Roe, S. et al., 2019: Contribution of the land sector to a 1.5°C world. *Nature Climate Change*, **9(11)**, 817–828, doi:10.1038/s41558-019-0591-9.

Roobaert, A., G.G. Laruelle, P. Landschützer, and P. Regnier, 2018: Uncertainty in the global oceanic CO_2 uptake induced by wind forcing: quantification and spatial analysis. *Biogeosciences*, **15(6)**, 1701–1720, doi:10.5194/bg-15-1701-2018.

Rosentreter, J.A., D.T. Maher, D. Erler, R.H. Murray, and B.D. Eyre, 2018: Methane emissions partially offset "blue carbon" burial in mangroves. *Science Advances*, **4(6)**, eaao4985, doi:10.1126/sciadv.aao4985.

Rubino, M. et al., 2019: Revised records of atmospheric trace gases CO_2, CH4, N2O, and 13C over the last 2000 years from Law Dome, Antarctica. *Earth System Science Data*, **11(2)**, 473–492, doi:10.5194/essd-11-473-2019.

Running, S. and M. Zhao, 2019: MOD17A3HGF MODIS/Terra Net Primary Production Gap-Filled Yearly L4 Global 500 m SIN Grid V006 [Data set]. NASA EOSDIS Land Processes DAAC.

Saeki, T. and P.K. Patra, 2017: Implications of overestimated anthropogenic CO_2 emissions on East Asian and global land CO_2 flux inversion. *Geoscience Letters*, **4(1)**, 9, doi:10.1186/s40562-017-0074-7.

Sallée, J.-B., R.J. Matear, S.R. Rintoul, and A. Lenton, 2012: Localized subduction of anthropogenic carbon dioxide in the Southern Hemisphere oceans. *Nature Geoscience*, **5(8)**, 579–584, doi:10.1038/ngeo1523.

Salter, I. et al., 2014: Carbonate counter pump stimulated by natural iron fertilization in the Polar Frontal Zone. *Nature Geoscience*, **7(12)**, 885–889, doi:10.1038/ngeo2285.

Saunois, M. et al., 2020: The Global Methane Budget 2000–2017. *Earth System Science Data*, **12(3)**, 1561–1623, doi:10.5194/essd-12-1561-2020.

Schilt, A. et al., 2010: Atmospheric nitrous oxide during the last 140,000years. *Earth and Planetary Science Letters*, **300(1–2)**, 33–43, doi:10.1016/j.epsl.2010.09.027.

Schwinger, J. et al., 2016: Evaluation of NorESM-OC (versions 1 and 1.2), the ocean carbon-cycle stand-alone configuration of the Norwegian Earth System Model (NorESM1). *Geoscientific Model Development*, **9(8)**, 2589–2622, doi:10.5194/gmd-9-2589-2016.

Seferian, R., 2018a: CNRM-CERFACS CNRM-ESM2-1 model output prepared for CMIP6 C4MIP 1pctCO_2-bgc. Earth System Grid Federation, doi:10.22033/esgf/cmip6.3717.

Seferian, R., 2018b: CNRM-CERFACS CNRM-ESM2-1 model output prepared for CMIP6 CMIP for experiment 1pctCO_2. Earth System Grid Federation, doi:10.22033/esgf/cmip6.3714.

Seferian, R., 2018c: CNRM-CERFACS CNRM-ESM2-1 model output prepared for CMIP6 CMIP historical. Earth System Grid Federation, doi:10.22033/esgf/cmip6.4068.

Seferian, R., 2018d: CNRM-CERFACS CNRM-ESM2-1 model output prepared for CMIP6 CMIP piControl. Earth System Grid Federation, doi:10.22033/esgf/cmip6.4165.

Seland et al., 2019: NCC NorESM2-LM model output prepared for CMIP6 CMIP historical. Earth System Grid Federation, doi:10.22033/esgf/cmip6.8036.

Shen, Q., M. Hedley, M. Camps Arbestain, and M.U.F. Kirschbaum, 2016: Can biochar increase the bioavailability of phosphorus? *Journal of Soil Science and Plant Nutrition*, **16(2)**, 268–286, doi:10.4067/s0718-95162016005000022.

Shutler, J.D. et al., 2016: FluxEngine: A Flexible Processing System for Calculating Atmosphere–Ocean Carbon Dioxide Gas Fluxes and Climatologies. *Journal of Atmospheric and Oceanic Technology*, **33(4)**, 741–756, doi:10.1175/jtech-d-14-00204.1.

Singh, N.K. et al., 2019: Optimizing wetland restoration to improve water quality at a regional scale. *Environmental Research Letters*, **14(6)**, 64006, doi:10.1088/1748-9326/ab1827.

Smetacek, V. et al., 2012: Deep carbon export from a Southern Ocean iron-fertilized diatom bloom. *Nature*, **487(7407)**, 313–319, doi:10.1038/nature11229.

Smith, P., J. Price, A. Molotoks, R. Warren, and Y. Malhi, 2018: Impacts on terrestrial biodiversity of moving from a 2°C to a 1.5°C target. *Philosophical*

Transactions of the Royal Society A: Mathematical, Physical and Engineering Sciences, **376(2119)**, 20160456, doi:10.1098/rsta.2016.0456.

Smith, P. et al., 2008: Greenhouse gas mitigation in agriculture. *Philosophical Transactions of the Royal Society B: Biological Sciences*, **363(1492)**, 789–813, doi:10.1098/rstb.2007.2184.

Smith, P. et al., 2016: Biophysical and economic limits to negative CO_2 emissions. *Nature Climate Change*, **6(1)**, 42–50, doi:10.1038/nclimate2870.

Smith, P. et al., 2019: Land-Management Options for Greenhouse Gas Removal and Their Impacts on Ecosystem Services and the Sustainable Development Goals. *Annual Review of Environment and Resources*, **44(1)**, 255–286, doi:10.1146/annurev-environ-101718-033129.

Smith, P. et al., 2020: Which practices co-deliver food security, climate change mitigation and adaptation, and combat land degradation and desertification? *Global Change Biology*, **26(3)**, 1532–1575, doi:10.1111/gcb.14878.

Smith, W.K., M. Zhao, and S.W. Running, 2012: Global bioenergy capacity as constrained by observed biospheric productivity rates. *BioScience*, **62(10)**, 911–922, doi:10.1525/bio.2012.62.10.11.

Sonntag, S. et al., 2018: Quantifying and Comparing Effects of Climate Engineering Methods on the Earth System. *Earth's Future*, **6(2)**, 149–168, doi:10.1002/2017ef000620.

Sutton, A.J. et al., 2014: Natural variability and anthropogenic change in equatorial Pacific surface ocean pCO_2 and pH. *Global Biogeochemical Cycles*, **28(2)**, 131–145, doi:10.1002/2013gb004679.

Sutton, A.J. et al., 2017: Variability and trends in surface seawater pCO_2 and CO_2 flux in the Pacific Ocean. *Geophysical Research Letters*, **44**, 5627–5636, doi:10.1002/2017gl073814.

Swart, N.C. et al., 2019a: CCCma CanESM5 model output prepared for CMIP6 C4MIP 1pctCO_2-bgc. Earth System Grid Federation, doi:10.22033/esgf/cmip6.3153.

Swart, N.C. et al., 2019b: CCCma CanESM5 model output prepared for CMIP6 CMIP 1pctCO_2. Earth System Grid Federation, doi:10.22033/esgf/cmip6.3151.

Swart, N.C. et al., 2019c: CCCma CanESM5 model output prepared for CMIP6 CMIP historical. Earth System Grid Federation, doi:10.22033/esgf/cmip6.3610.

Swart, N.C. et al., 2019d: CCCma CanESM5 model output prepared for CMIP6 CMIP piControl. Earth System Grid Federation, doi:10.22033/esgf/cmip6.3673.

Swart, N.C. et al., 2019e: CCCma CanESM5 model output prepared for CMIP6 ScenarioMIP ssp126. Earth System Grid Federation, doi:10.22033/esgf/cmip6.3683.

Swart, N.C. et al., 2019f: CCCma CanESM5 model output prepared for CMIP6 ScenarioMIP ssp245. Earth System Grid Federation, doi:10.22033/esgf/cmip6.3685.

Swart, N.C. et al., 2019g: CCCma CanESM5 model output prepared for CMIP6 ScenarioMIP ssp370. Earth System Grid Federation, doi:10.22033/esgf/cmip6.3690.

Swart, N.C. et al., 2019h: CCCma CanESM5 model output prepared for CMIP6 ScenarioMIP ssp534-over. Earth System Grid Federation, doi:10.22033/esgf/cmip6.3694.

Swart, N.C. et al., 2019i: CCCma CanESM5 model output prepared for CMIP6 ScenarioMIP ssp585. Earth System Grid Federation, doi:10.22033/esgf/cmip6.3696.

Sweeney, C. et al., 2007: Constraining global air-sea gas exchange for CO_2 with recent bomb 14C measurements. *Global Biogeochemical Cycles*, **21(2)**, GB2015, doi:10.1029/2006gb002784.

Tachiiri, K. et al., 2019a: MIROC MIROC-ES2L model output prepared for CMIP6 ScenarioMIP ssp126. Earth System Grid Federation, doi:10.22033/esgf/cmip6.5742.

Tachiiri, K. et al., 2019b: MIROC MIROC-ES2L model output prepared for CMIP6 ScenarioMIP ssp245. Earth System Grid Federation, doi:10.22033/esgf/cmip6.5745.

Tachiiri, K. et al., 2019c: MIROC MIROC-ES2L model output prepared for CMIP6 ScenarioMIP ssp370. Earth System Grid Federation, doi:10.22033/esgf/cmip6.5751.

Tachiiri, K. et al., 2019d: MIROC MIROC-ES2L model output prepared for CMIP6 ScenarioMIP ssp585. Earth System Grid Federation, doi:10.22033/esgf/cmip6.5770.

Takahashi, T. et al., 2014: Climatological distributions of pH, pCO_2, total CO_2, alkalinity, and CaCO3 saturation in the global surface ocean, and temporal changes at selected locations. *Marine Chemistry*, **164**, 95–125, doi:10.1016/j.marchem.2014.06.004.

Tang, Y. et al., 2019a: MOHC UKESM1.0-LL model output prepared for CMIP6 CMIP 1pctCO_2. Earth System Grid Federation, doi:10.22033/esgf/cmip6.5792.

Tang, Y. et al., 2019b: MOHC UKESM1.0-LL model output prepared for CMIP6 CMIP historical. Earth System Grid Federation, doi:10.22033/esgf/cmip6.6113.

Tang, Y. et al., 2019c: MOHC UKESM1.0-LL model output prepared for CMIP6 CMIP piControl. Earth System Grid Federation, doi:10.22033/esgf/cmip6.6298.

Tanhua, T. et al., 2017: Temporal changes in ventilation and the carbonate system in the Atlantic sector of the Southern Ocean. *Deep Sea Research Part II: Topical Studies in Oceanography*, **138**, 26–38, doi:10.1016/j.dsr2.2016.10.004.

Tatebe, H. and M. Watanabe, 2018: MIROC MIROC6 model output prepared for CMIP6 CMIP historical. Earth System Grid Federation, doi:10.22033/esgf/cmip6.5603.

Thompson, R.L. et al., 2019: Acceleration of global N2O emissions seen from two decades of atmospheric inversion. *Nature Climate Change*, **9(12)**, 993–998, doi:10.1038/s41558-019-0613-7.

Tian, H. et al., 2019: Global soil nitrous oxide emissions since the preindustrial era estimated by an ensemble of terrestrial biosphere models: Magnitude, attribution, and uncertainty. *Global Change Biology*, **25(2)**, 640–659, doi:10.1111/gcb.14514.

Tian, H. et al., 2020: A comprehensive quantification of global nitrous oxide sources and sinks. *Nature*, **586(7828)**, 248–256, doi:10.1038/s41586-020-2780-0.

Tohjima, Y., H. Mukai, T. Machida, Y. Hoshina, and S.-I. Nakaoka, 2019: Global carbon budgets estimated from atmospheric O2/N2 and\n$CO_2$ observations in the western Pacific region over a 15-year period. *Atmospheric Chemistry and Physics*, **19(14)**, 9269–9285, doi:10.5194/acp-19-9269-2019.

Tokarska, K.B. and K. Zickfeld, 2015: The effectiveness of net negative carbon dioxide emissions in reversing anthropogenic climate change. *Environmental Research Letters*, **10(9)**, 094013, doi:10.1088/1748-9326/10/9/094013.

Tonitto, C., M.B. David, and L.E. Drinkwater, 2006: Replacing bare fallows with cover crops in fertilizer-intensive cropping systems: A meta-analysis of crop yield and N dynamics. *Agriculture, Ecosystems & Environment*, **112(1)**, 58–72, doi:10.1016/j.agee.2005.07.003.

Toyama, K. et al., 2017: Large reemergence of anthropogenic carbon into the ocean's surface mixed layer sustained by the ocean's overturning circulation. *Journal of Climate*, **30(21)**, 8615–8631, doi:10.1175/jcli-d-16-0725.1.

Tsuruta, A. et al., 2017: Global methane emission estimates for 2000–2012 from CarbonTracker Europe-CH4 v1.0. *Geoscientific Model Development*, **10(3)**, 1261–1289, doi:10.5194/gmd-10-1261-2017.

Tucker, C.J. et al., 2005: An extended AVHRR 8-km NDVI dataset compatible with MODIS and SPOT vegetation NDVI data. *International Journal of Remote Sensing*, **26(20)**, 4485–4498, doi:10.1080/01431160500168686.

Turnbull, J.C. et al., 2017: Sixty years of radiocarbon dioxide measurements at Wellington, New Zealand: 1954–2014. *Atmospheric Chemistry and Physics*, **17(23)**, 14771–14784, doi:10.5194/acp-17-14771-2017.

van der Laan-Luijkx, I.T. et al., 2017: The CarbonTracker Data Assimilation Shell (CTDAS) v1.0: implementation and global carbon balance 2001–

2015. *Geoscientific Model Development*, **10(7)**, 2785–2800, doi:10.5194/gmd-10-2785-2017.

Verheijen, F.G.A. et al., 2019: The influence of biochar particle size and concentration on bulk density and maximum water holding capacity of sandy vs sandy loam soil in a column experiment. *Geoderma*, **347**, 194–202, doi:10.1016/j.geoderma.2019.03.044.

Voldoire, A., 2019a: CNRM-CERFACS CNRM-ESM2-1 model output prepared for CMIP6 ScenarioMIP ssp126. Earth System Grid Federation, doi:10.22033/esgf/cmip6.4186.

Voldoire, A., 2019b: CNRM-CERFACS CNRM-ESM2-1 model output prepared for CMIP6 ScenarioMIP ssp245. Earth System Grid Federation, doi:10.22033/esgf/cmip6.4191.

Voldoire, A., 2019c: CNRM-CERFACS CNRM-ESM2-1 model output prepared for CMIP6 ScenarioMIP ssp370. Earth System Grid Federation, doi:10.22033/esgf/cmip6.4199.

Voldoire, A., 2019d: CNRM-CERFACS CNRM-ESM2-1 model output prepared for CMIP6 ScenarioMIP ssp585. Earth System Grid Federation, doi:10.22033/esgf/cmip6.4226.

Wakita, M., A. Nagano, T. Fujiki, and S. Watanabe, 2017: Slow acidification of the winter mixed layer in the subarctic western North Pacific. *Journal of Geophysical Research: Oceans*, **122(8)**, 6923–6935, doi:10.1002/2017jc013002.

Wang, F. et al., 2019: Methane Emission Estimates by the Global High-Resolution Inverse Model Using National Inventories. *Remote Sensing*, **11(21)**, 2489, doi:10.3390/rs11212489.

Wang, S. et al., 2019: A 2-year study on the effect of biochar on methane and nitrous oxide emissions in an intensive rice–wheat cropping system. *Biochar*, **1(2)**, 177–186, doi:10.1007/s42773-019-00011-8.

Wanninkhof, R., 1992: Relationship between wind speed and gas exchange over the ocean. *Journal of Geophysical Research: Oceans*, **97(C5)**, 7373–7382, doi:10.1029/92jc00188.

Wanninkhof, R., 2014: Relationship between wind speed and gas exchange over the ocean revisited. *Limnology and Oceanography: Methods*, **12(6)**, 351–362, doi:10.4319/lom.2014.12.351.

Weiss, R.F., 1974: Carbon dioxide in water and seawater: the solubility of a non-ideal gas. *Marine Chemistry*, **2(3)**, 203–215, doi:10.1016/0304-4203(74)90015-2.

White, J.W.C., B.H. Vaughn, and S.E. Michel, 2018: Stable Isotopic Composition of Atmospheric Methane (13C) from the NOAA ESRL Carbon Cycle Cooperative Global Air Sampling Network, 1998-2017, Version: 2018-09-24. University of Colorado, Institute of Arctic and Alpine Research (INSTAAR).

Wieners, K.-H. et al., 2019a: MPI-M MPI-ESM1.2-LR model output prepared for CMIP6 ScenarioMIP ssp126. Earth System Grid Federation, doi:10.22033/esgf/cmip6.6690.

Wieners, K.-H. et al., 2019b: MPI-M MPI-ESM1.2-LR model output prepared for CMIP6 ScenarioMIP ssp245. Earth System Grid Federation, doi:10.22033/esgf/cmip6.6693.

Wieners, K.-H. et al., 2019c: MPI-M MPI-ESM1.2-LR model output prepared for CMIP6 ScenarioMIP ssp370. Earth System Grid Federation, doi:10.22033/esgf/cmip6.6695.

Wieners, K.-H. et al., 2019d: MPI-M MPI-ESM1.2-LR model output prepared for CMIP6 ScenarioMIP ssp585. Earth System Grid Federation, doi:10.22033/esgf/cmip6.6705.

Wieners, K.-H. et al., 2019e: MPI-M MPI-ESM1.2-LR model output prepared for CMIP6 CMIP 1pctCO_2. Earth System Grid Federation, doi:10.22033/esgf/cmip6.6435.

Wieners, K.-H. et al., 2019f: MPI-M MPI-ESM1.2-LR model output prepared for CMIP6 CMIP historical. Earth System Grid Federation, doi:10.22033/esgf/cmip6.6595.

Wieners, K.-H. et al., 2019g: MPI-M MPI-ESM1.2-LR model output prepared for CMIP6 CMIP piControl. Earth System Grid Federation, doi:10.22033/esgf/cmip6.6675.

Williams, N.L. et al., 2017: Calculating surface ocean pCO_2 from biogeochemical Argo floats equipped with pH: An uncertainty analysis. *Global Biogeochemical Cycles*, **31(3)**, 591–604, doi:10.1002/2016gb005541.

Williamson, P. and R. Bodle, 2016: *Update on Climate Geoengineering in Relation to the Convention on Biological Diversity: Potential Impacts and Regulatory Framework*. Secretariat of the Convention on Biological Diversity, Montreal, QC, Canada, 158 pp.

Williamson, P. et al., 2012: Ocean fertilization for geoengineering: A review of effectiveness, environmental impacts and emerging governance. *Process Safety and Environmental Protection*, **90(6)**, 475–488, doi:10.1016/j.psep.2012.10.007.

Wilson, D. et al., 2016a: Greenhouse gas emission factors associated with rewetting of organic soils. *Mires and Peat*, **17(04)**, 1–28, doi:10.19189/map.2016.omb.222.

Wilson, D. et al., 2016b: Multiyear greenhouse gas balances at a rewetted temperate peatland. *Global Change Biology*, **22(12)**, 4080–4095, doi:10.1111/gcb.13325.

Wolter, K. and M.S. Timlin, 1998: Measuring the strength of ENSO events: How does 1997/98 rank? *Weather*, **53(9)**, 315–324, doi:10.1002/j.1477-8696.1998.tb06408.x.

Wolter, K. and M.S. Timlin, 2011: El Niño/Southern Oscillation behaviour since 1871 as diagnosed in an extended multivariate ENSO index (MEI.ext). *International Journal of Climatology*, **31(7)**, 1074–1087, doi:10.1002/joc.2336.

Woolf, D., J.E. Amonette, F.A. Street-Perrott, J. Lehmann, and S. Joseph, 2010: Sustainable biochar to mitigate global climate change. *Nature Communications*, **1(1)**, 56, doi:10.1038/ncomms1053.

Worrall, F. et al., 2019: The Impact of Peatland Restoration on Local Climate: Restoration of a Cool Humid Island. *Journal of Geophysical Research: Biogeosciences*, **124(6)**, 1696–1713, doi:10.1029/2019jg005156.

Wu, T. et al., 2018: BCC BCC-CSM2MR model output prepared for CMIP6 CMIP historical. Earth System Grid Federation, doi:10.22033/esgf/cmip6.2948.

Xue, L. et al., 2014: Temporal changes in surface partial pressure of carbon dioxide and carbonate saturation state in the eastern equatorial Indian Ocean during the 1962–2012 period. *Biogeosciences*, **11(22)**, 6293–6305, doi:10.5194/bg-11-6293-2014.

Yang, S. et al., 2019: Biochar improved rice yield and mitigated CH4 and N2O emissions from paddy field under controlled irrigation in the Taihu Lake Region of China. *Atmospheric Environment*, **200**, 69–77, doi:10.1016/j.atmosenv.2018.12.003.

Yin, Y. et al., 2015: Decadal trends in global CO emissions as seen by MOPITT. *Atmospheric Chemistry and Physics*, **15(23)**, 13433–13451, doi:10.5194/acp-15-13433-2015.

Yoshida, Y. et al., 2013: Improvement of the retrieval algorithm for GOSAT SWIR XCO_2 and XCH4 and their validation using TCCON data. *Atmospheric Measurement Techniques*, **6(6)**, 1533–1547, doi:10.5194/amt-6-1533-2013.

Zeng, J., Y. Nojiri, P. Landschützer, M. Telszewski, and S. Nakaoka, 2014: A Global Surface Ocean fCO_2 Climatology Based on a Feed-Forward Neural Network. *Journal of Atmospheric and Oceanic Technology*, **31(8)**, 1838–1849, doi:10.1175/jtech-d-13-00137.1.

Zhang, J. et al., 2019: BCC BCC-CSM2MR model output prepared for CMIP6 GMMIP hist-resIPO. Earth System Grid Federation, doi:10.22033/esgf/cmip6.2934.

Zhang, Y., J. Joiner, S. Hamed Alemohammad, S. Zhou, and P. Gentine, 2018a: A global spatially contiguous solar-induced fluorescence (CSIF) dataset using neural networks. *Biogeosciences*, **15(19)**, doi:10.5194/bg-15-5779-2018.

Zhang, Y. et al., 2018b: Response of surface albedo and soil carbon dioxide fluxes to biochar amendment in farmland. *Journal of Soils and Sediments*, **18(4)**, 1590–1601, doi:10.1007/s11368-017-1889-8.

Zickfeld, K., D. Azevedo, S. Mathesius, and H.D. Matthews, 2021: Asymmetry in the climate–carbon cycle response to positive and negative CO_2 emissions. *Nature Climate Change*, **11(7)**, 613–617, doi:10.1038/s41558-021-01061-2.

Ziehn, T. et al., 2019a: CSIRO ACCESS-ESM1.5 model output prepared for CMIP6 C4MIP 1pctCO_2-bgc. Earth System Grid Federation, doi:10.22033/esgf/cmip6.4232.
Ziehn, T. et al., 2019b: CSIRO ACCESS-ESM1.5 model output prepared for CMIP6 CMIP 1pctCO_2. Earth System Grid Federation, doi:10.22033/esgf/cmip6.4231.
Ziehn, T. et al., 2019c: CSIRO ACCESS-ESM1.5 model output prepared for CMIP6 CMIP historical. Earth System Grid Federation, doi:10.22033/esgf/cmip6.4272.
Ziehn, T. et al., 2019d: CSIRO ACCESS-ESM1.5 model output prepared for CMIP6 CMIP piControl. Earth System Grid Federation, doi:10.22033/esgf/cmip6.4312.
Ziehn, T. et al., 2019e: CSIRO ACCESS-ESM1.5 model output prepared for CMIP6 ScenarioMIP ssp126. Earth System Grid Federation, doi:10.22033/esgf/cmip6.4320.
Ziehn, T. et al., 2019f: CSIRO ACCESS-ESM1.5 model output prepared for CMIP6 ScenarioMIP ssp245. Earth System Grid Federation, doi:10.22033/esgf/cmip6.4322.
Ziehn, T. et al., 2019g: CSIRO ACCESS-ESM1.5 model output prepared for CMIP6 ScenarioMIP ssp370. Earth System Grid Federation, doi:10.22033/esgf/cmip6.4324.
Ziehn, T. et al., 2019h: CSIRO ACCESS-ESM1.5 model output prepared for CMIP6 ScenarioMIP ssp585. Earth System Grid Federation, doi:10.22033/esgf/cmip6.4333.